

UC Irvine

UC Irvine Previously Published Works

Title

Vulnerability in a Tropical Cyclone Risk Model: Philippines Case Study

Permalink

<https://escholarship.org/uc/item/39p941st>

Journal

Weather Climate and Society, 15(3)

ISSN

1948-8327

Authors

Baldwin, Jane W

Lee, Chia-Ying

Walsh, Brian J

et al.

Publication Date

2023-07-01

DOI

10.1175/wcas-d-22-0049.1

Copyright Information

This work is made available under the terms of a Creative Commons Attribution License, available at <https://creativecommons.org/licenses/by/4.0/>

Peer reviewed

Vulnerability in a Tropical Cyclone Risk Model: Philippines Case Study

JANE W. BALDWIN^{a,b}, CHIA-YING LEE,^b BRIAN J. WALSH,^c SUZANA J. CAMARGO,^b AND ADAM H. SOBEL^d

^a *Department of Earth System Science, University of California, Irvine, Irvine, California*

^b *Lamont-Doherty Earth Observatory, Palisades, New York*

^c *World Bank, Washington, D.C.*

^d *Columbia University, New York, New York*

(Manuscript received 10 April 2022, in final form 15 February 2023, accepted 21 February 2023)

ABSTRACT: The authors describe a tropical cyclone risk model for the Philippines using open-source methods that can be straightforwardly generalized to other countries. Wind fields derived from historical observations, as well as those from an environmentally forced tropical cyclone hazard model, are combined with data representing exposed value and vulnerability to determine asset losses. Exposed value is represented by the LitPop dataset, which assumes total asset value is distributed across a country following population density and night-lights data. Vulnerability is assumed to follow a functional form previously proposed by Emanuel, with free parameters chosen by a sensitivity analysis in which simulated and historical reported damages are compared for different parameter values and further constrained by information from household surveys about regional building characteristics. Use of different vulnerability parameters for the region around Manila, Philippines, yields much better agreement between simulated and actually reported losses than does a single set of parameters for the entire country. Despite the improvements from regionally refined vulnerability, the model predicts no losses for a substantial number of destructive historical storms, a difference the authors hypothesize is due to the use of wind speed as the sole metric of tropical cyclone hazard, omitting explicit representation of storm surge and/or rainfall. Bearing these limitations in mind, this model can be used to estimate return levels for tropical cyclone–caused wind hazards and asset losses for regions across the Philippines, relevant to some disaster risk reduction and management tasks; this model also provides a platform for further development of open-source tropical cyclone risk modeling.

SIGNIFICANCE STATEMENT: Landfalling tropical cyclones are devastating disasters for which the Philippines is particularly at risk. Here we develop a model for tropical cyclone risk, quantified as property losses, over the Philippines and demonstrate its effectiveness by comparing to historical damages. We find that capturing the difference in vulnerability between the largest city in the Philippines (Manila) and more rural areas is important to accurately represent this risk. Using this model, we can more accurately constrain the risk of very extreme tropical cyclone events in the Philippines. The model can also be straightforwardly adapted for emergency planning in other countries and for climate change scenarios using openly available information.


KEYWORDS: Hurricanes/typhoons; Tropical cyclones; Emergency preparedness; Risk assessment; Societal impacts; Vulnerability

1. Introduction

Accurate assessments of tropical cyclone (TC) risk are valuable for disaster risk reduction and climate adaptation. Such assessments can inform decisions about both where to build resilience and emergency preparedness prior to TC-induced disasters and where to allocate aid following such disasters; they can also inform the development of insurance and reinsurance products. Assessing risk requires consideration of three different factors (Field et al. 2012). The first factor is the hazard, the

probabilities that given levels of geophysical variables (e.g., wind speed, rainfall, storm surge) will be exceeded. The second factor is the exposure, which characterizes the human, structural, or agricultural assets in a place that might be affected by the disaster. The third factor is the vulnerability, which is the degree to which those assets will be lost if one or more of the geophysical variables exceeds a given value. TC risks are typically quantified in the form of asset losses, or the replacement cost of assets destroyed by a TC event.

Over the past decade or so, significant strides have been made in quantifying different aspects of TC risk. Given that TCs—particularly the few most-intense ones that cause the largest share of damage—are rare events, the observed historical record is too limited for accurate TC risk assessment. Statistical–dynamical models have been developed that allow the simulation of many physically plausible TCs given background environmental conditions (Emanuel et al. 2008; Lee et al. 2018; Jing and Lin 2020; Bloemendaal et al. 2020b). Synthetic TCs generated by such models are used for assessment of extreme wind hazards (Emanuel 2011; Sobel et al. 2019;

 Denotes content that is immediately available upon publication as open access.

 Supplemental information related to this paper is available at the Journals Online website: <https://doi.org/10.1175/WCAS-D-22-0049.s1>.

Corresponding author: Jane W. Baldwin, jane.baldwin@uci.edu

DOI: 10.1175/WCAS-D-22-0049.1

© 2023 American Meteorological Society. For information regarding reuse of this content and general copyright information, consult the [AMS Copyright Policy \(www.ametsoc.org/PUBSReuseLicenses\)](https://www.ametsoc.org/PUBSReuseLicenses).

Bloemendaal et al. 2020a; Lee et al. 2022), coupled with hydrodynamical models to estimate storm surge hazards (Lin et al. 2010; Lin and Chavas 2012) and with physics-based models of precipitation to estimate extreme rainfall hazards (Xi et al. 2020; Gori et al. 2022). A key challenge for TC risk assessment is incorporating changing hazards following climate change. Traditionally, hurricane risk assessment has been based primarily on historical tracks (Watson and Johnson 2004), but this approach is not appropriate in a nonstationary climate. In contrast, the statistical-dynamical approaches can be applied with environmental conditions drawn from climate change scenarios to estimate changing hazards from TCs (Emanuel et al. 2008; Lee et al. 2020).

Alongside these advances in modeling TC hazards, progress has been made in modeling TC vulnerability and exposure. This work can be broadly categorized into structural, economic, and social approaches (Wilson et al. 2022). For the United States, FEMA's Hazus model provides a relatively comprehensive framework for modeling wind and flood risks, including computation of exposure and vulnerability from building maps and structural engineering principles (Vickery et al. 2006b,a). Some information in Hazus, especially around vulnerability of building types, has been adapted for use in other countries by the United Nations International Strategy for Disaster Reduction (UNISDR)'s Global Assessment Reports (Yamin et al. 2014). However, the lack of detailed building maps and the complexity of Hazus limit its applicability to other countries. In contrast, recent studies using top-down, economic-based approaches have created global exposure fields and country-scale impact functions for TC risk modeling (Geiger et al. 2018; Eberenz et al. 2020, 2021). While these methods are more simplified than Hazus, they have the advantage of being consistently applicable across the globe. Vulnerability can also be estimated based on population characteristics (what we term "social approaches"; e.g., Cutter et al. 2003; Tellman et al. 2020; Dominguez et al. 2021). While these techniques are suitable for assessing relative vulnerabilities of different regions (e.g., counties), existing social approaches are somewhat less straightforward to merge with TC hazard and exposure for quantitative risk assessment.

The primary goal of the present work is to develop open-source methods for assessing tropical cyclone risk that are applicable to lower-income nations with relatively limited data. To do so requires the development of layers for hazard, exposure, and vulnerability using public data sources and open-source code. We develop and validate our TC risk model around the Philippines as a case study but pursue methods that can be straightforwardly repurposed for other countries. In particular, we develop layers for vulnerability and exposure to combine with TC tracks from the Columbia Tropical Cyclone Hazard (CHAZ) model, as well as with tracks from historical observations. CHAZ is a statistical-dynamical tropical cyclone model that can generate many physically plausible synthetic TCs based on background environmental conditions, allowing evaluation of TC risks for longer return periods than are available from the historical record alone (Lee et al. 2018). Importantly for this work, CHAZ code is open source, and the performance of CHAZ is comparable to that of other stochastic TC hazard models, including in the

western North Pacific (Meiler et al. 2022). For exposure, we employ an existing global dataset of asset value called LitPop that depends on population and night-lights data (Eberenz et al. 2020). Finally, for vulnerability we fit parameters for an existing vulnerability function (Emanuel 2011) at the regional level by combining information on damages and wind swaths for historical TCs with survey data on household construction materials. Vulnerability is the component of the model that is least constrained by existing observational data and therefore was a substantial focus of our research.

The secondary goal of this work is to produce and validate a TC risk model for the Philippines that is usable for some disaster risk reduction and management tasks. This project was a collaboration between climate scientists and economists at the World Bank. The World Bank and other nonprofit organizations regularly use information about TC and other disaster risks in planning distribution of postdisaster aid and investments in disaster resilience. While proprietary data from catastrophe modeling companies can constrain TC risk in the Philippines, these sources often stop short of providing spatially resolved maps of losses, which are useful for accurate distribution of aid. The financial costs associated with such proprietary data also often make it infeasible to test assumptions in the risk modeling process. Thus, our work seeks to develop and document a model for TC risk in the Philippines that might fill these gaps and be usable by the World Bank and other nonprofit applications. The model described here extends a prior open-source model that conducted country-scale analyses of TC vulnerability (Eberenz et al. 2021) but struggled to accurately capture risk in the Philippines. We demonstrate that varying vulnerability by administrative districts (i.e., regions) substantially improves the accuracy of TC risk estimates in the Philippines. In summary, while our model is less refined than proprietary risk models based on claims data, we aim to take a useful step forward in open-source TC risk modeling and provide a platform for future model development.

The rest of this paper is structured as follows. Section 2 provides background on the geography of the Philippines and storms affecting this country. Section 3 describes the methods and datasets used in this work. Section 4 shows the sensitivity of risk estimates to different assumptions about vulnerability. Section 5 applies this risk model to create TC risk estimates for the Philippines based on CHAZ. Section 6 discusses demonstrated capabilities and uncertainties/limitations of our modeling approach. Finally, section 7 ends this paper with a summary and conclusions. The supplemental material is referenced throughout the paper and provides additional model validation and details relevant but less central to the main manuscript.

2. The Philippines context

In this study, we focus on TC risk assessment for the Philippines largely because this country experiences particularly high risks from these events. About 70% of western North Pacific typhoons form in or enter the region directly surrounding the Philippines (Corporal-Lodangco and Leslie 2017). The more active period for TCs is June–December, during which time the median number of landfalls in the Philippines is six (Corporal-Lodangco and

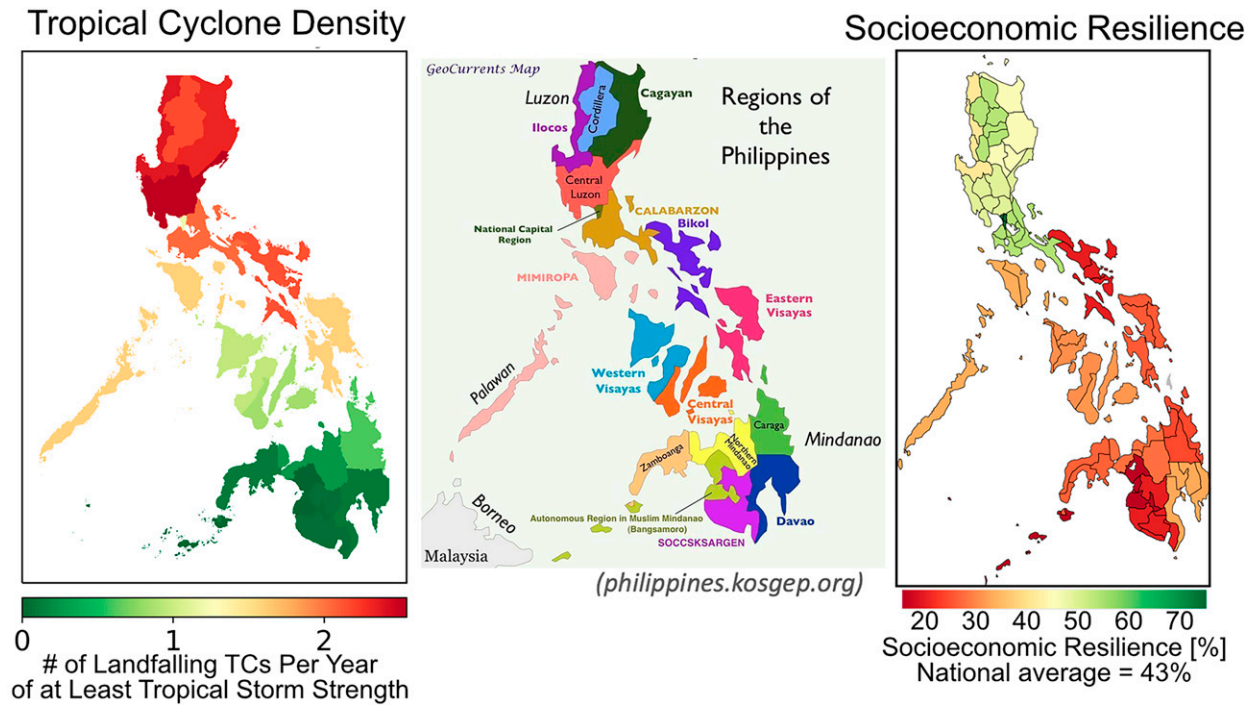


FIG. 1. Contrasting TC density and socioeconomic resilience in the northern vs southern Philippines. (left) Number of TCs and typhoons per year making landfall in different regions of the Philippines; (center) Regions in the Philippines (adapted from philippines.kosgep.org); (right) average socioeconomic resilience in different regions of the Philippines. Socioeconomic resilience is defined here as the ratio of expected asset losses to wellbeing losses in Walsh and Hallegatte (2020), from which the right panel is adapted. Wellbeing losses are calculated using household survey data about consumption habits across the Philippines.

Leslie 2017). Around the Philippines, ENSO plays a dominant role in year-to-year variability of TC genesis frequency, tracks, and associated precipitation (Lyon and Camargo 2009; Corporal-Lodangco et al. 2016) and has been implicated in the formation of exceedingly strong storms (Lin et al. 2014).

Landfalling typhoons in the Philippines are disasters both in terms of economic impacts and fatalities (Ribera et al. 2008; Walsh and Hallegatte 2019). Recent storms have highlighted these dangers. In 2013, Typhoon Haiyan made landfall in the Philippines as a category 5 storm, but with maximum sustained winds exceeding the threshold for category 5 by over 18 m s^{-1} (Lin et al. 2014). The extremely strong winds were accompanied by very high-velocity surges and resultant flooding (Soria et al. 2016). The storm made a direct hit to Eastern Visayas, a region on the eastern side of the Philippines. Haiyan is estimated to have cost the Philippines more than \$10 billion (Ehrhart et al. 2014) and resulted in 6300 known fatalities, the vast majority occurring in Eastern Visayas, with an additional 1062 individuals missing and 28 688 injured (del Rosario 2013). These impacts were exacerbated by large populations living along the coast in structurally vulnerable (wood or bamboo) housing (Mas et al. 2015; Eadie et al. 2020). For perspective, Hurricane Katrina resulted in 1833 known fatalities and several hundred persons missing in the United States (Beven et al. 2008). Very recently, in December 2021, Typhoon Rai (Odette) made multiple landfalls in the southern Philippines with an initial intensity of category 5, causing widespread flooding. This disaster is the third-costliest

typhoon in Philippines history, affecting an estimated 12 million people and causing more than 400 fatalities (United Nations Office for the Coordination of Humanitarian Affairs 2022).

There is a strong need for accurate TC risk assessment in the Philippines to support disaster risk reduction and management efforts. However, assessment of TC risk in the Philippines is complicated by opposing spatial gradients of hazard and socioeconomic vulnerability (Fig. 1). The northern Philippines experiences more frequent TCs than does the southern Philippines but is also wealthier and more socioeconomically resilient, i.e., better able to cope with and recover from disaster asset losses. The city of Manila and its surroundings [also called the National Capital Region (NCR)], constitute by far the most populated and developed region in the Philippines. In contrast, the southern Philippines is generally poorer and less socioeconomically resilient. Socioeconomic resilience is defined here as the ratio of expected asset losses to wellbeing losses, as in Walsh and Hallegatte (2020). These opposing patterns of hazard and resilience pose a dilemma for the Philippines itself and international agencies (such as the World Bank) aiming to distribute aid for disaster risk reduction. Should this aid focus on the northern Philippines, where exposure and hazards, and in turn asset losses, are greatest, or on the southern Philippines, which is more vulnerable and where the human wellbeing losses may be greatest? To answer this question requires rigorous TC risk assessment that accurately models differences in losses across the Philippines, and, ultimately, consideration of losses across the income distribution.

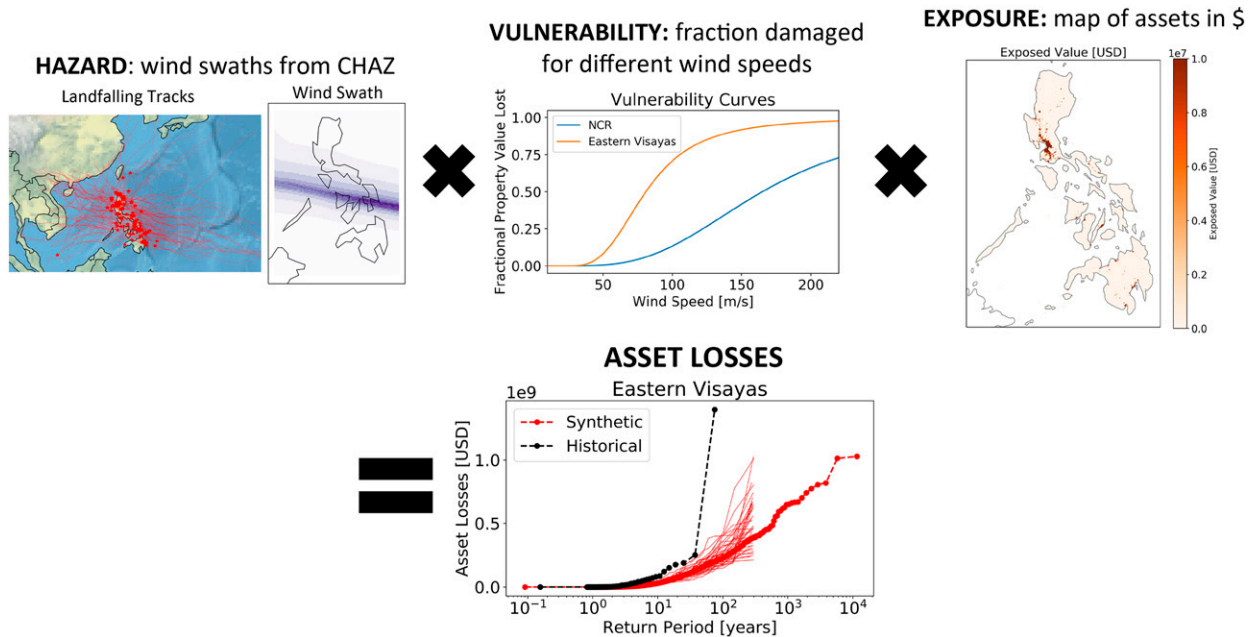


FIG. 2. Schematic of our TC risk modeling workflow. Layers for hazard, vulnerability, and exposed value are combined to model asset losses from TCs. Details of each layer are described in section 3.

In the Philippines, “region” is the name for a particular administrative division; the country is divided into 17 regions (Fig. 1; center panel), which are further subdivided into 81 provinces. For some results, we focus on two regions as contrasting examples: 1) the NCR, which contains Manila and is highly urbanized, and 2) Eastern Visayas, a relatively less-affluent region that was directly impacted by Typhoon Haiyan.

3. Methods

Our workflow combines hazard, vulnerability, and exposure to calculate asset losses from TCs in the Philippines (Fig. 2) and validates those asset losses against observations from historical storms. We describe the basic methods we use to determine each risk component separately here and discuss vulnerability further in the next section.

a. Hazard

We make the simplifying assumption that total TC losses can be modeled as a function of wind speed. In reality, TCs cause losses through a number of different additional subperils associated with these events, including intense rainfall, storm surge, and associated flooding and landslides (Cinco et al. 2016). Rainfall and storm surge are only indirectly and loosely related to wind speed; for example, some relatively weak but slow-moving storms can result in large amounts of rainfall (Sato and Nakasu 2011). However, due to additional complexities involved in modeling rainfall and storm surge, wind speed alone is often used as a first-order estimate of TC hazard (Eberenz et al. 2021; Geiger et al. 2018; Emanuel 2011).

We use two different types of TC track data. The first comprises historical TC tracks from the International Best Track

Archive for Climate Stewardship, v04r00 (IBTrACS). This version includes data from a number of different meteorological agencies across the world (Knapp et al. 2010). Given that multiple agencies may provide track and intensity data for a particular storm, we choose to examine western North Pacific track data from only the Joint Typhoon Warning Center (JTWC). Philippines-landfalling storms recorded in this dataset span from 1945 to the present. The second data source consists of synthetic tracks from CHAZ, specifically those produced using environmental fields from the ERA-Interim reanalysis (Dee et al. 2011; Lee et al. 2018). Both the historical and CHAZ tracks are available at 6-hourly temporal resolution. We extract the salient information from these tracks (latitude, longitude, maximum sustained wind speed) and linearly interpolate them to a 15-min temporal resolution. We use tracks that make landfall in the Philippines, determined by the intersection of these 15-min-temporal-resolution track points with a 5-arc-minute-spatia-resolution land mask of this country. In IBTrACS, there are 480 historical Philippines-landfalling tropical cyclones. Downscaled from ERA-Interim, CHAZ generated in total 94 500 synthetic storms making landfall in the Philippines. This number includes 3178 storm tracks, and each track has roughly 30 stochastically generated intensification trajectories (Lee et al. 2016, 2018). For each of these landfalling storms, we use data extending from 1 day before the first landfall to 1 day after the last landfall in the Philippines for our risk analysis. Samples of landfalling TC tracks from IBTrACS and CHAZ are shown in Fig. 3. Across the two sets of TCs, locations of landfall and distribution of intensities at first landfall are similar. However, CHAZ synthetic TCs do not last as long after passing through the Philippines as IBTrACS-observed TCs, which may be related

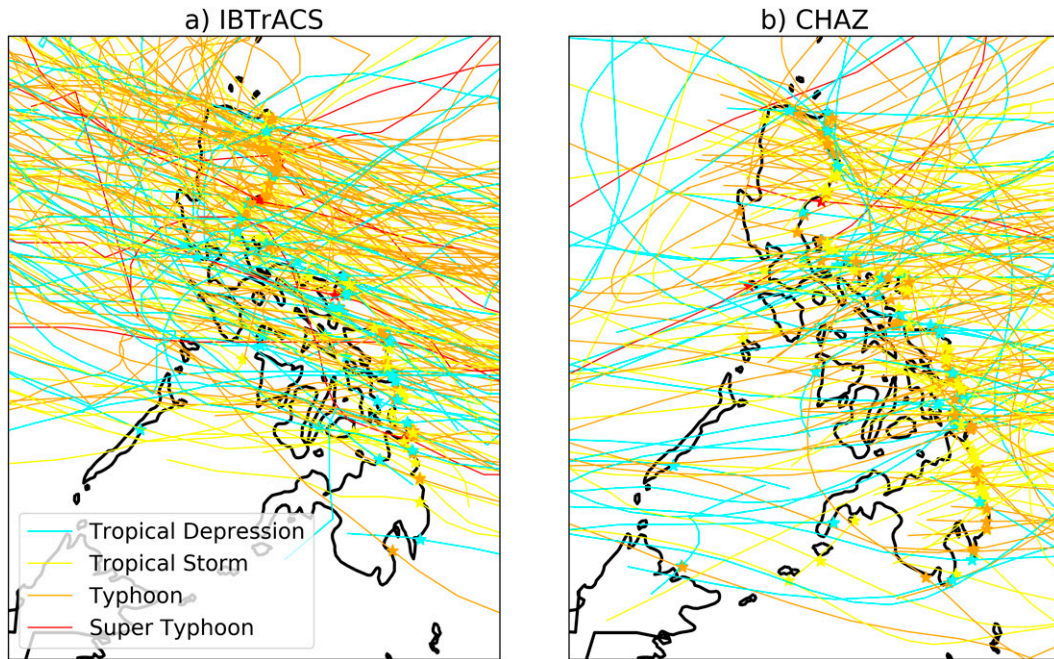


FIG. 3. Example of observed vs synthetic landfalling TCs. Sample of 200 landfalling TC tracks from (a) IBTrACS and (b) CHAZ. First landfall in the Philippines is demarcated with a star, and tracks are shaded by intensity at first landfall.

to post-landfall decay assumptions in CHAZ, and are directed more southward.

A TC track consists of a set of points defining a one-dimensional curve in time and space, with wind represented by a single number, the maximum sustained wind speed. It is necessary to generate two-dimensional wind swaths at each point along the track, in order to use those winds, together with spatially varying exposure and vulnerability data, to model damage. Swaths should account for the variation of wind speed from the center of the storm and some asymmetries typical in TCs. To do this, we employ an approach based on previously published parametric wind models, described below and summarized in Fig. 4. An important input to this modeling approach is the radius of maximum wind (RMW). In IBTrACS, observed estimates of RMW are available for some storms but not all. As a result, we estimate RMW using the empirically derived Knaff et al. (2015) formula, in which the predicted RMW depends on latitude and maximum sustained wind speed. This formula was developed using data from the North Atlantic basin, where storms typically do not reach intensities as high as those in the western North Pacific basin. A side effect of this difference is that the formula produces physically unreasonable RMW values (extremely small or negative) for the strongest storms observed around the Philippines. To compensate for this issue, any RMW values predicted by the formula to be less than 20 km are overridden to be 20 km, which is on the lower end of the observed RMW distribution, similar to what is seen for high-intensity storms (Hsu and Yan 1998).

Once we have calculated an RMW for each storm at each 15-min time step, we can determine an associated radial profile of the azimuthal wind (Fig. 4). Various parametric TC

wind profile models exist (Chavas et al. 2015; Willoughby et al. 2006; Holland 1980); in all of them, azimuthal wind speed increases with radius from the eye of the storm until the RMW, at which value it begins to decrease with radius. We elect to use Willoughby et al. (2006), as it performs comparably well or slightly better than other wind profile models when compared to satellite-based observations of hurricane wind fields (Yang et al. 2022). Inputs to this model are RMW, maximum sustained wind speed, and latitude, and the shape is determined by an empirically fit double exponential profile.

The next step is to convert the one-dimensional radial profiles to two-dimensional wind swaths on a latitude–longitude grid. As we do this, we add a representation of asymmetry due to the translation of the storm along its track, which accelerates winds on the side of the storm where the storm-relative azimuthal velocity is in the same direction as the storm translation and decelerates them on the opposite side (Klotz and Jiang 2017; Uhlhorn et al. 2014). We first construct a $0.1^\circ \times 0.1^\circ$ rectilinear grid spanning the Philippines. We then determine the track translation speed V and track direction Θ from a forward difference of the time step of interest and the subsequent time step. The azimuthal velocity at each grid point imposed by the translation of the storm can then be calculated as follows:

$$\theta_{i,j} = \arctan2[(y_{i,j} - Y), (x_{i,j} - X)] - \Theta, \quad (1)$$

$$v_{t(i,j)} = -V \times \cos(\pi/2 - \theta_{i,j}), \quad (2)$$

where X and Y are the longitude and latitude locations of the storm center, x and y are the longitude and latitude values for each point (i, j) on the grid, θ is the angle relative to the track

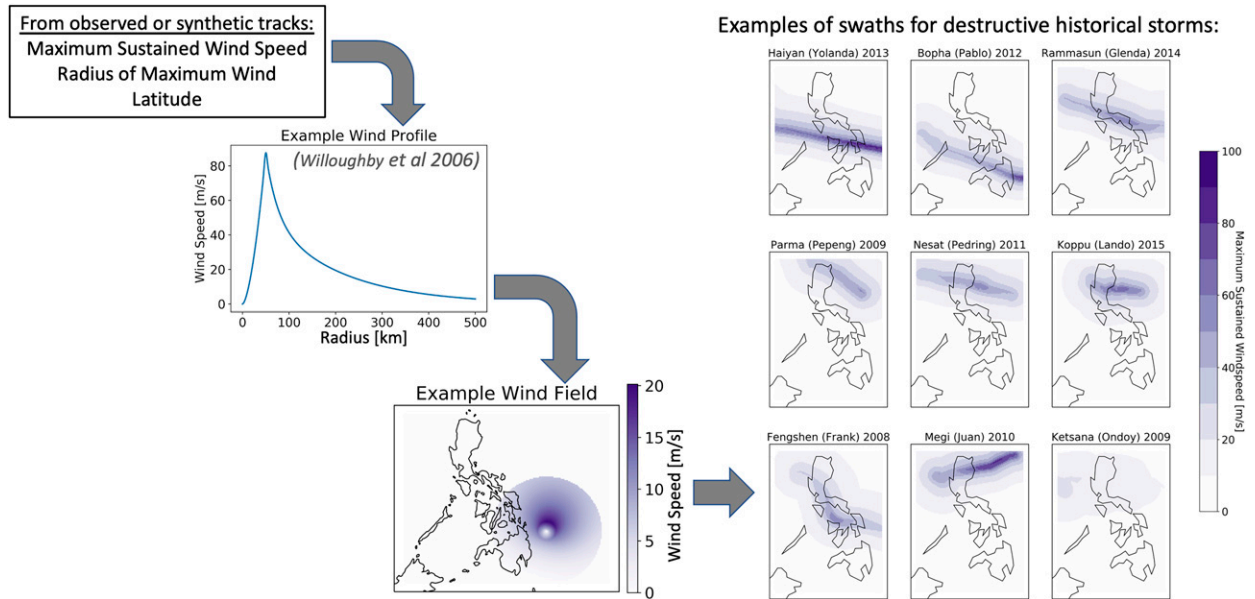


FIG. 4. Wind swath calculation schematic and resulting swaths for highly destructive historical TCs. (left to right) 1) Information on maximum sustained wind speed, latitude, and RMW along TC tracks is used to determine 2) profiles of wind with radius from the center of the storm, which is 3) placed on a latitude–longitude grid and combined with a correction for asymmetry to determine wind fields at each point in time, then 4) the wind swath is determined as the maximum across time of the wind fields when the storm is near land. Swaths corresponding to nine of the costliest historical storms affecting the Philippines are shown on the right-hand side of the figure.

direction at each location (i, j) on the grid, and v_t is the imposed azimuthal velocity from the storm translation at each point (i, j) on the grid.

Applying a large asymmetry correction far from the storm center can result in winds that increase with radius in some directions, a feature we view as unrealistic. Thus, we modulate v_t based on distance from the storm center before applying it to the wind field,

$$\alpha_{i,j}[r_{i,j} \geq 1] = e^{-0.314-0.042r_{i,j}}, \quad (3)$$

$$\alpha_{i,j}[r_{i,j} < 1] = 0.3r_{i,j} + 0.4, \quad (4)$$

$$v_{a(i,j)} = \alpha_{i,j}v_{t(i,j)}, \quad (5)$$

where r is the radius from the center of the storm in kilometers normalized by the RMW (so $r = 1$ at the RMW), α is the factor modulating the asymmetry correction, and v_a is the asymmetry correction; α is designed assuming that the impact of the storm motion on the symmetric background wind is reduced with radius. The above equation gives us maximum asymmetries imposed by translation speed at the RMW with $\alpha = 0.7$, gradually decreasing to 0.3 outward. These values of α are within a rough range of the estimated values of storm translation to surface background wind reduction factor shown in Lin and Chavas (2012).

The final wind field is determined by regridding the Willoughby et al. (2006) radial wind profile to the latitude–longitude grid and adding the asymmetry correction $[v_{a(i,j)}]$. To this end, to ensure the maximum wind speed remains unchanged, we input to the

wind profile calculation the maximum sustained wind speed minus the maximum asymmetry correction $[\max(v_a) = 0.7\max(v_r)]$. Once a wind field is determined for each 15-min time step of a given storm, the final wind swath to be used in loss calculations is obtained by taking the maximum of all the wind fields across time at each latitude–longitude grid point. Examples of resulting wind swaths for nine of the most destructive historical storms in the Philippines are shown in Fig. 4.

Above, we presented a relatively simple construction of two-dimensional wind swaths that captures storm wind at first order and allows efficient generation of wind maps for large numbers of synthetic storms. Despite its relative simplicity, our parametric wind fields and swaths reasonably capture the magnitude and structure of observation-derived products (see Figs. 1–3 in the supplemental material and related text). Our method is also similar in construction and complexity to that of other open-source tropical cyclone exposure modeling efforts, notably Geiger et al. (2018), which conducted a larger-scale wind field validation exercise. Given encouraging results from these validation exercises, and results in a prior study indicating that wind speed exceedance curves were relatively insensitive to alternative possible choices for the parametric wind field modeling (Lee et al. 2022), we conclude our wind fields are sufficiently accurate for the present risk modeling exercise.

That said, there are a variety of ways in which this wind field construction could be improved. For example, one can use a more sophisticated method in estimating RMW (Chavas and Knaff 2022) and adding asymmetries (Lin and Chavas 2012; Chang et al. 2020; Yang et al. 2022). Additionally,

following landfall, another significant source of asymmetry in the wind field is the roughness of the land surface (e.g., buildings, plants, and topography), which generally decelerates wind speeds. For our initial model described here, we neglect this roughness effect. This will lead to overestimates of the wind over land, but we view this as an acceptable compromise for the level of analysis we conduct here, particularly because the vulnerability curves are calibrated to these winds. Incorporating roughness and conducting a detailed optimization of wind field modeling for the Philippines are out of scope for the present study, which focuses primarily on exploring methods for vulnerability assessment in this region. However, they are areas we hope to pursue in future work.

b. Exposure

We represent exposure via a global dataset of assets in U.S. dollars across space developed by Eberenz et al. (2020). This dataset, called LitPop, is constructed by disaggregating 2014 national total asset value across space proportionally to population density and night-lights data. The national total asset value data used are the World Bank's produced capital stock, which represents the value of manufactured or built assets in each country, not including the value of agricultural products (World Bank 2021). The night-lights data used are NASA's Black Marble nighttime lights (Román et al. 2018), and the population data used are the Gridded Population of the World (Doxsey-Whitfield et al. 2015). Validating by disaggregating national GDP and comparing to regional GDP estimates in 14 countries, Eberenz et al. (2020) finds that disaggregating proportionally to LitPop¹ (where Lit is the night-lights data and Pop is the population data, and the numbers designate powers that the data are raised to) likely provides the best estimate of asset distribution. It is worth noting that the validation exercise was performed in a set of 14 countries that did not include the Philippines. An improved Philippines-specific dataset might be constructed by fitting this dataset for the Philippines and perhaps considering the distribution of agricultural products across space. But we expect that the existing dataset provides a reasonable-enough estimate of asset distribution for this initial risk model. In the Philippines, LitPop shows by far the highest asset density in and around Manila, with more minor hot spots of asset concentration in other major cities (Fig. 5).

LitPop is available at a relatively high 30-arc-s resolution, which is equivalent to the resolution of the underlying population data. To allow the wind hazard to interact with exposure, we bilinearly interpolate the $0.1^\circ \times 0.1^\circ$ wind swaths to the higher resolution of the LitPop data. This is done to leverage the spatial detail in the exposure dataset.

c. Vulnerability

Vulnerability is the propensity of exposed value to be destroyed in the face of a geophysical hazard (Wilson et al. 2022). In the context of our model, vulnerability converts a given wind speed to percentage of assets destroyed. Intuitively, at low-to-moderate wind speeds, such as those that are commonly experienced in the absence of a tropical cyclone, no damage should occur, and at high wind speeds, damages

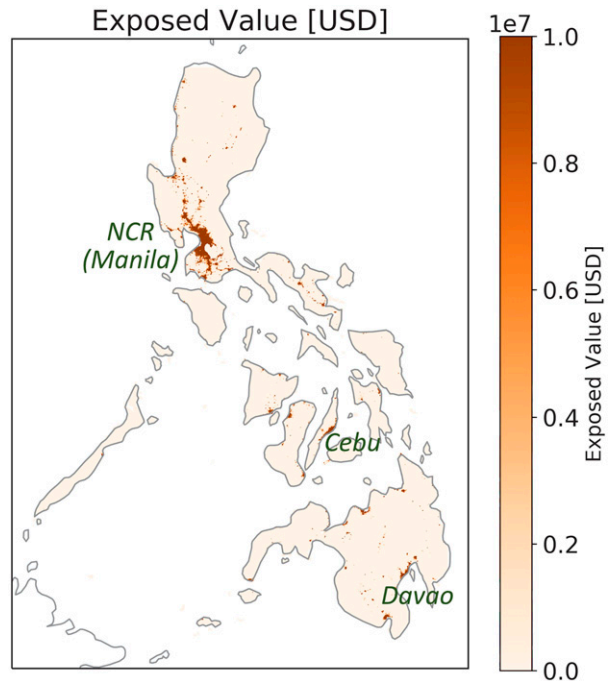


FIG. 5. Asset value across the Philippines according to LitPop. Shaded is the estimated value of assets in 2014 U.S. dollars for each 30-arc-s grid cell of LitPop. Major cities with high concentrations of assets are labeled.

should increase until they saturate at 100% of exposed value. There are a few different functional forms for TC wind-related vulnerability (called impact functions, vulnerability curves, or damage functions) that have been proposed. Here we use the functional form presented in Emanuel (2011), which is structured as follows:

$$f = \frac{v_n^3}{1 + v_n^3}, \quad (6)$$

$$v_n = \frac{\max[(V - V_{\text{thresh}}), 0]}{V_{\text{half}} - V_{\text{thresh}}}, \quad (7)$$

where f is the fraction of the asset value lost, V is the wind speed, V_{thresh} is the wind speed at and below which no damage occurs, and V_{half} is the wind speed at which half the asset value is lost (Fig. 6). The third power of wind speed in Eq. (6) is based on physical arguments (Emanuel 2005) and empirical analysis, i.e., regression against historical losses in the United States (Strobl 2011). In the function shown in Eq. (7), the parameters V_{thresh} and V_{half} determine vulnerability—lower values of these parameters correspond to higher vulnerability. We note that V_{thresh} is necessarily always lower than V_{half} .

The vulnerability function above was developed to represent damage from extreme wind, but has been used to predict total TC-related damages in various applications. Most relevant to this study, Eberenz et al. (2021; hereafter ELB21) fit country-wide impact functions to simulate total historical TC damages in different countries, including the Philippines. In

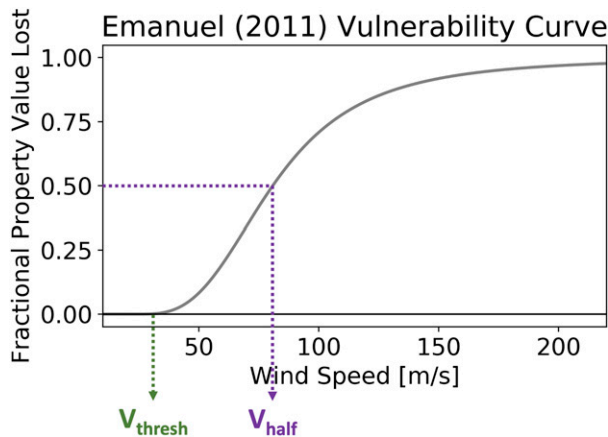


FIG. 6. Example vulnerability curve based on Emanuel (2011). Indicated are the two parameters that constrain the vulnerability curve: V_{thresh} (the minimum wind speed to have any damages) and V_{half} (the wind speed at which 50% of property value is lost).

that study, the values of V_{half} are varied to optimally simulate total damages, while V_{thresh} is kept constant at 25.7 m s^{-1} (50 kt), an approach that has been used and to some degree supported in other studies. For example, in Emanuel (2011) this 25.7 m s^{-1} V_{thresh} value was proposed for the United States, while the value of V_{half} varied in order to represent different vulnerability levels, and this same V_{thresh} value is somewhat consistent with structural vulnerability curves for wind used in the Hazus risk modeling framework (Vickery et al. 2006b). This approach of varying V_{half} but not V_{thresh} has also been shown to reasonably simulate losses in China (Elliott et al. 2015). Since there is rather limited justification of this V_{thresh} value when using wind as a proxy for all damages, and it is plausible that lower V_{thresh} values may be justified to the extent that nonwind hazards (such as flooding) are being implicitly represented, we examine sensitivity of our risk results to both V_{half} and V_{thresh} .

Our process for fitting this vulnerability function for the Philippines is discussed in more detail in section 4. A dataset we use in this fitting process is the Family Income and Expenditure Survey (FIES) for the Philippines. FIES is conducted by the Filipino government's National Statistics Office and is a key tool for poverty quantification (Erica and Fabian 2009). It surveys tens of thousands of households in the Philippines on diverse and detailed aspects of their incomes, spending, and saving. Particularly relevant here, it also includes information on their dwellings. This survey is completed every 3 years. We employ 2015 data on dwelling construction materials (Bersales 2017). The FIES categorizes roof and wall construction materials into seven different categories, which can roughly be ordered from weakest to strongest. As discussed below, we employ this data as a proxy for TC structural vulnerability.

d. Reported damage data

To develop and validate our risk model, we compare our results to estimates of historical losses from real TCs that have affected the Philippines. For this purpose, we use the

Emergency Events Database (EM-DAT), which aggregates data on a wide range of disasters (Guha-Sapir et al. 2009). EM-DAT includes disasters from 1900 to the present that meet one of the following criteria: 10 or more people dead, 100 or more people affected, the declaration of a state of emergency, and/or a call for international assistance. Sources of data included in EM-DAT vary, but priority is given to information from United Nations (UN) agencies, governments, and the International Federation of Red Cross and Red Crescent Societies. From EM-DAT, we select only data entries for storms affecting the Philippines and use the start date, end date, and total damages for each storm. We retain storms that have damage estimates, start and end dates, and are not labeled as convective or extratropical events (260 events total). While tropical cyclones are convective in nature, all events with the convective label in Philippines EM-DAT are either tornados or related to frontal systems, hence their exclusion from our analysis. Of the 260 included events, 245 are labeled as TCs. The event names of the remaining 15 indicate that these are tropical depressions or tropical storms—we also include these in our analysis, as they were TCs but just did not have typhoon intensity at the time of landfall in the Philippines. The timing of these events spans 1952 to the present (Fig. 7). Their associated losses span many orders of magnitude, with the smallest loss for an individual TC event being \$5,000 and the greatest loss \$10 billion, caused by Typhoon Haiyan.

The number of events included in the dataset also increases over time—this may result from changes in observing practices or actual increases in TC risk caused by population growth and development and/or changes in TC characteristics (in particular TC intensity) due to anthropogenic climate change (Knutson et al. 2020). Here we evaluate the model by comparing simulated damages to those in EM-DAT event by event, without explicitly considering when each event occurred, so any changes in observing practices are effectively random errors for our purpose. The possible effects of such changes would have to be considered more explicitly if one wished to study temporal trends in damage.

e. Comparison between reported and simulated damages

To reasonably compare EM-DAT with our simulated damages, we need to account for change in assets over time and inflation. However, the LitPop dataset uses asset data from 2014, while the damage values in EM-DAT should be compared to asset values at the time the event occurred. Therefore, in order to reasonably compare simulated and observed damages, we first normalize the observed damages to 2014 values via the Penn World Tables' (version 10.0) quantification of Philippines capital stock, which is closely related to total asset value (Feenstra et al. 2015) and provided in units of constant 2017 national prices in dollars. Specifically, we follow a procedure similar to that in ELB21:

$$\text{NRD}_E = \text{RD}_E \frac{\text{CS}_{2014}}{\text{CS}_y}, \quad (8)$$

where E represents a particular event, y is the year the event occurs, RD is the raw reported damages, NRD is normalized

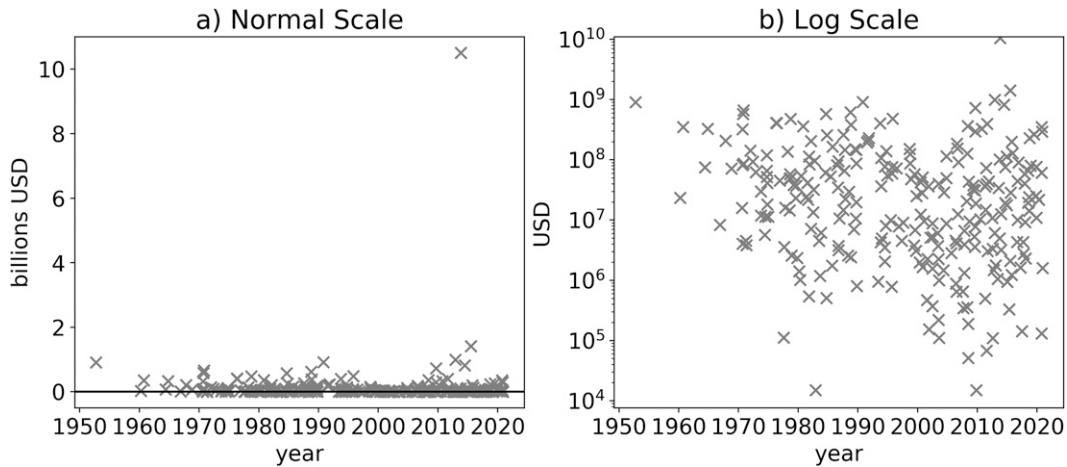


FIG. 7. Historical TC-related damages for the Philippines over time from EM-DAT with (a) a linear y axis and (b) a log-scale y axis, highlighting the many orders of magnitude that damages from these events span.

reported damages, and CS is capital stock. For the rest of this paper, “reported damages” refers to damages normalized this way.

EM-DAT presents damages in entire country totals. For some events, additional information is provided specifying the region affected, but the lack of consistency in this information makes it difficult to employ in our analysis. As such, in validating simulated damages against reported damages, we always first sum all simulated damages across the Philippines.

To pair simulated to reported damages, we need a way of identifying corresponding events in EM-DAT and IBTrACS. In theory, the events could be paired based on storm names and years (e.g., Haiyan in 2013). However, we found that slight variations in the names made this method difficult. Instead, we pair the simulated losses to reported losses using the dates of occurrence of the events, similar to ELB21. Sometimes event dates overlap (e.g., two events share 3–6 August 2018), but typically events do not share all the same dates (e.g., one event spans 1–7 August while the other spans 2–6 August). Thus, we pair an EM-DAT and an IBTrACS event if their dates overlap for the largest number of days compared to any other possible pairings. Using this method results in 134 unambiguous matches. There were five ambiguous matches that required special considerations, which are detailed in the supplemental material. Many storms are excluded because there is an IBTrACS track but no overlapping EM-DAT damage event or vice versa. Altogether, this process results in matches for 139 events.

We use a few different metrics to compare reported and simulated damages. Three are standard metrics of correlation: Pearson’s r , Kendall’s τ , and Spearman’s r . Pearson’s r measures the linear correlation between two datasets, whereas Kendall’s τ and Spearman’s r are both nonparametric, rank-based correlation coefficients—they assess the extent to which one dataset is a monotonic function of the other. For all three of these metrics, model performance is better when the correlation is closer to 1. The two additional metrics are drawn from ELB21 and reflect distinct needs in developing a TC risk

model. The first metric is the total damage ratio (TDR), and is quantified as

$$TDR = \frac{\sum_{E=1}^N SD_E}{\sum_{E=1}^N NRD_E}, \quad (9)$$

where E from 1 to N spans all the relevant historical TC events, NRD is the normalized reported damages, and SD is our model’s simulated damages. A TDR of 1 is optimal. TDR reflects the ability of our risk model to simulate total damages across all events and is dominated by the events that cause the greatest asset losses (e.g., Haiyan). However, as discussed further in section 4, lack of skill in simulating more moderate events can be masked by TDR. To better assess skill across a range of events, ELB21 also introduces a metric called root-mean-squared fraction (RMSF), which is quantified as

$$RMSF = \exp \left\{ \sqrt{\frac{1}{N} \sum_{E=1}^N [\ln(EDR_E)]^2} \right\}, \quad (10)$$

where EDR stands for event damage ratio and is defined as SD_E/NRD_E for any given event. RMSF weighs errors proportionally to event magnitude, so that a 50% error (for example) is equally important, whether it is 50% of a small or large loss. Values of RMSF closer to 1 represent lower model errors. TDR and RMSF reflect different considerations relevant to development of a TC risk model. Ideally, a model would perform well for both metrics, but in general (and in our results below) there are trade-offs such that prioritizing one versus the other implies different modeling choices.

4. Development of the vulnerability layer

In this section, we estimate vulnerability across space in the Philippines, which we call a vulnerability layer, to be combined with hazard and exposure to estimate Philippines TC

risk. In developing a vulnerability layer, our general approach is to determine which vulnerability parameter values result in the best match between reported damages and simulated damages for historical TCs. As mentioned above, we only consider TCs that make landfall in the Philippines (excluding near misses) and are included in EM-DAT. Fitting vulnerability to damages as described here is primarily an empirical approach, though we note that the Emanuel (2011) vulnerability curve functional form we employ is also informed by the physics of wind-driven damage. Below, we describe a couple of specific methods for fitting vulnerability in the Philippines with varying levels of spatial complexity.

a. National fit

We initially apply the same vulnerability curve for all locations in the Philippines. This is similar to the approach employed in ELB21, who notably found very different values for V_{half} in the Philippines depending on whether TDR or RMSF was optimized, which were 188.4 and 84.7 m s^{-1} , respectively. Using these V_{half} values and the V_{thresh} value used in ELB21 (25.7 m s^{-1}) as a starting point, we test the sensitivity of simulated damages to V_{half} and V_{thresh} . Specifically, we evaluate simulated damages for V_{half} every 10 m s^{-1} between 50 and 200 m s^{-1} and for V_{thresh} every 5 m s^{-1} between 15 and 35 m s^{-1} . For each combination of these parameter values, we calculate the various correlation metrics described in section 3 comparing simulated versus reported damages (supplemental Fig. 4). This sensitivity analysis highlights the difficulty of confidently fitting a single vulnerability curve for the Philippines. Depending on the correlation metric examined, very different parameter values are found to be optimal. Not only that, but the structure of the dependence of the correlation metrics on the two vulnerability parameters varies substantially (see the supplemental material for further description of this sensitivity analysis and comparison of our national fit vulnerability results to ELB21).

For the rest of the paper, we simplify our vulnerability-fitting procedure in a few ways for parsimony and consistency with prior work. First, we focus on optimizing TDR and RMSF, which we believe are more intuitive to interpret than the other correlation metrics for emergency planning and preparedness. Second, rather than continuing to fit V_{thresh} and V_{half} , we hold V_{thresh} constant at 25 m s^{-1} (approximately the same value as ELB21) and vary only V_{half} . As measured by TDR and RMSF, the degree of agreement with observed damages can be fit to some extent either by V_{thresh} or V_{half} (supplemental Figs. 4d,e); focusing on V_{half} seems a reasonable simplifying assumption, especially as we have a somewhat stronger a priori constraint on V_{thresh} (i.e., that it should be somewhere near the low end of the maximum sustained wind speeds found in tropical storms). However, we emphasize that the sensitivity analysis shown in supplemental Fig. 4 cannot clearly exclude values of V_{thresh} greater or lower than 25 m s^{-1} . Unlike prior work that has stated that V_{thresh} is relatively well constrained to be around 25 m s^{-1} (Emanuel 2011; Elliott et al. 2015), our analysis suggests further examination of appropriate V_{thresh} values is warranted, particularly in contexts where, as here, wind is being used as a proxy for all

damages, rather than modeling only damages directly caused by wind.

Figure 8 plots reported damages against simulated damages for historical TCs, with the vulnerability parameter set to the optimal RMSF fit when holding V_{thresh} constant at 25 m s^{-1} ($V_{\text{half}} = 80 \text{ m s}^{-1}$). When RMSF is minimized, TDR is 9.28—meaning total simulated damages are about 9 times greater than those reported. This suggests a significant trade-off between capturing the damages for individual storms and across all storms when applying one vulnerability curve for the entire Philippines. To better understand the cause of this overestimation of total damages, we assessed possible commonalities among outliers. We found that storms passing through the large, urban capital region, including Manila, by and large exhibited overestimated simulated damages. This is shown in Fig. 8a by the blue-circled values climbing the y axis (simulated damages) for very low reported damages values, in Fig. 8b by all the blue-circled values lying above the black one-to-one line, and in Fig. 8c by storms that pass through Manila disproportionately exhibiting high event-damage ratios. Figure 8c is very similar to and inspired by Fig. 7 in ELB21, though we find more storms with event-damage ratios less than 0.1 than did those authors, as we include storms where simulated damages are 0.

These results seem to reflect the limitations of country-scale vulnerability in capturing significant urban–rural differences. Manila is much more built up and wealthier than other regions in the Philippines, with likelier lower vulnerability (though greater exposure). As a result, when a vulnerability curve fit for the entire Philippines is employed to calculate damages for a storm passing through Manila, damages are overestimated. Our hypothesis is that developing a more spatially detailed map of vulnerability in the Philippines would better capture these urban–rural differences and allow more accurate simulation of damages for individual storms (i.e., lower RMSF) and across all storms (i.e., TDR closer to 1).

b. Regional fit

Motivated by the results above, we develop a vulnerability layer with spatial variability in the vulnerability parameters. To capture a very high level of spatial detail, one might match buildings across the Philippines with building-type specific vulnerability curves similar to the methodology used for the United States in FEMA's Hazus (Vickery et al. 2006b). However, this approach requires a detailed map of building types across the Philippines, which we lack. Instead, we take an intermediate approach between a single, empirically derived vulnerability curve for all the Philippines (the approach used in the previous section) and a building-level map of structural vulnerability to develop a region-scale TC vulnerability layer for the Philippines.

Our first step is to fit V_{half} for each region in the Philippines that has historically been damaged by TCs. A challenge here is that EM-DAT only provides nationally aggregated damage estimates. In lieu of region-level damage data, we fit V_{half} for each region based on the subset of historical storms that result in positive simulated asset losses for that region. Given the

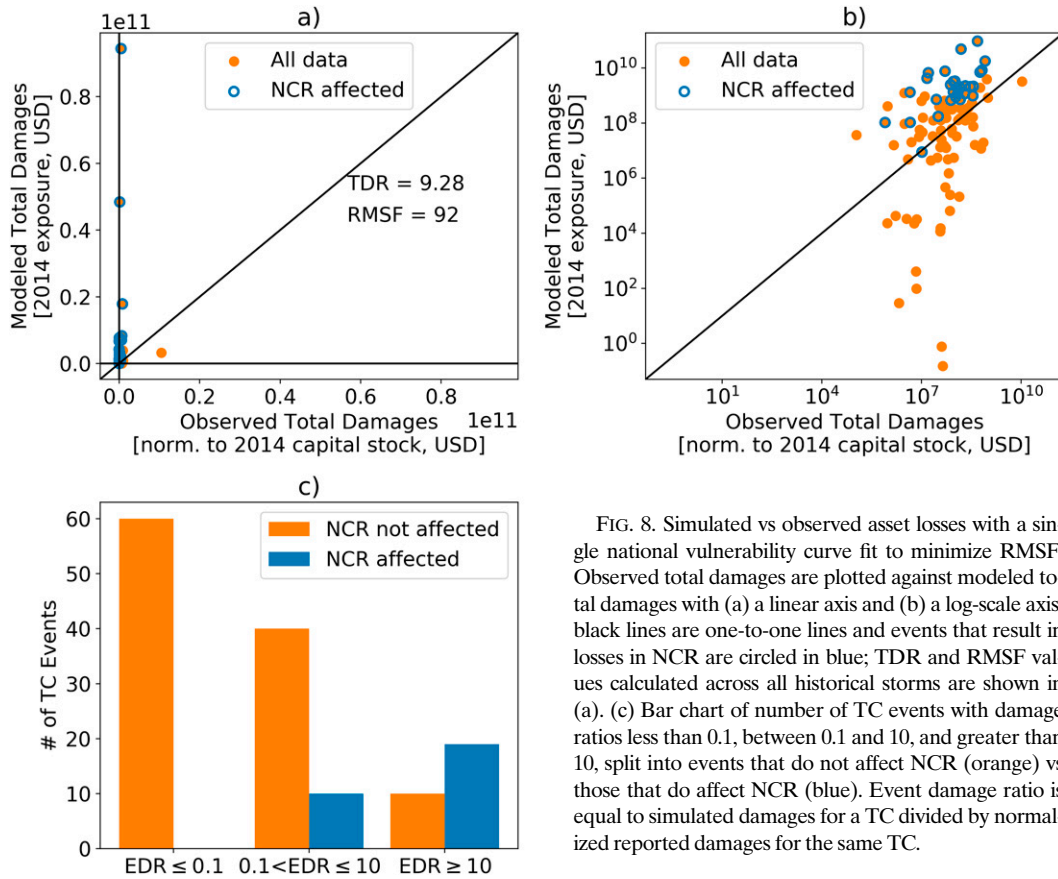


FIG. 8. Simulated vs observed asset losses with a single national vulnerability curve fit to minimize RMSF. Observed total damages are plotted against modeled total damages with (a) a linear axis and (b) a log-scale axis; black lines are one-to-one lines and events that result in losses in NCR are circled in blue; TDR and RMSF values calculated across all historical storms are shown in (a). (c) Bar chart of number of TC events with damage ratios less than 0.1, between 0.1 and 10, and greater than 10, split into events that do not affect NCR (orange) vs those that do affect NCR (blue). Event damage ratio is equal to simulated damages for a TC divided by normalized reported damages for the same TC.

limitations of EM-DAT, we also compare the national sum of reported damages to simulated damages, but just for the subset of storms affecting a given region. The assumption here is that even though the damage estimate for any given storm may be affected by neighboring regions impacted by the same TC, in aggregate across all historical storms this subset should reflect the TC risk for the region of interest. We then determine the V_{half} values that minimize RMSF for storms affecting each region. For most regions, V_{half} ranges from 60 to 120 $m s^{-1}$. Manila, as predicted, exhibits lower vulnerability than any other region, with an optimal V_{half} equal to 180 $m s^{-1}$.

Because some regions of the Philippines have been affected by very few storms in the historical record, it is highly uncertain or impossible to fit V_{half} using the method described above for every region. For example, the Autonomous Region in Muslim Mindanao (ARMM) has experienced zero recorded landfalling storms according to our analysis of IBTrACS. To create a vulnerability map consistent across the Philippines, and also lend further confidence to our vulnerability quantification, we employ on-the-ground data about structural vulnerability included in the FIES. The FIES surveys a sample of households and groups them by region, making it possible to derive region-scale information. The FIES includes information on both roof and wall construction materials. We focus on roof materials, as both full-scale and wind-tunnel-model studies and post-TC damage surveys indicate

that this is the most wind-vulnerable part of a house (Holmes 1982; Meecham et al. 1991; Leitch et al. 2010; Jayasinghe et al. 2018), and structural damage often occurs through damage to the roof allowing rain to enter a building (D. Rowe 2021, personal communication). The roof materials listed in the FIES dataset fall into seven categories (supplemental Fig. 5). Most roofs are categorized as “strong material (galvanized, iron,

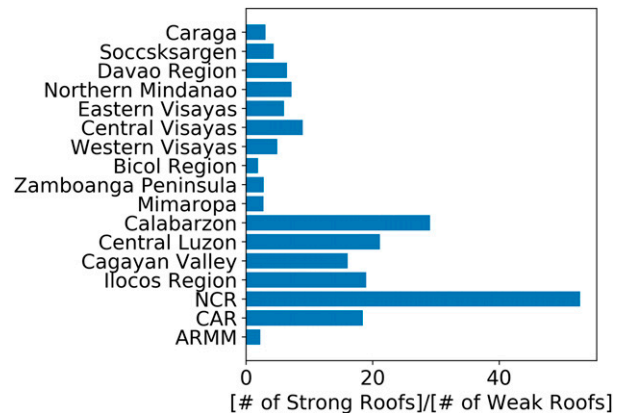


FIG. 9. Proportion of strong to weak roofs for regions in the Philippines. Bar chart showing number of strong roofs divided by number of light roofs for each region in the Philippines.

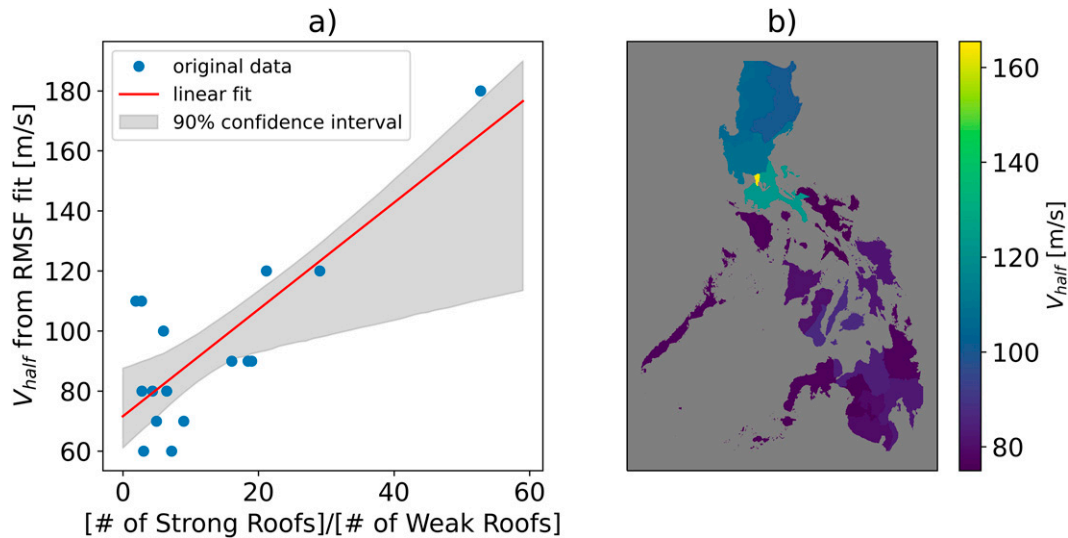


FIG. 10. Correspondence of regional V_{half} to roof strength proportion and resulting vulnerability map from regression. (a) Proportion of strong to weak roofs plotted against RMSF-fitted regional V_{half} values (blue circles) and linear fit between the two quantities (red line) with a bootstrapped 90% confidence interval of the linear fit (gray shading); (b) regional V_{half} determined from proportion of strong to weak roofs in each province and linear fit in (a). Note that in (a), NCR is the top-right point in the plot with the highest V_{half} and highest proportion of strong roofs.

al[uminum], tile, concrete, brick, stone, asbestos)” or “light material (cogon, nipa, *anahaw*.” Cogon, nipa, and *anahaw* are plant materials used to make straw thatch roofs. We use the ratio of strong to light roof materials as a proxy for structural vulnerability (Fig. 9). As might be expected, NCR has the highest proportion of strong to light roofs, whereas a more rural and impoverished region such as Eastern Visayas has a much lower proportion of strong to light roofs.

We hypothesize that the proportion of strong to light roofs influences TC vulnerability and should positively correlate with the V_{half} value fit in different regions. Indeed, we find a positive association between these two quantities (Fig. 10a;

NCR is the top-right point). This association likely reflects the direct impact of roof strength on TC damages, as well as other socioeconomic factors such as income and extent of the social safety net, which partially correlate with construction quality and influence disaster outcomes. We linearly regress the proportion of strong to light roofs against V_{half} and use the resulting regression coefficients and regional values of the roof proportion to calculate a final V_{half} value for each region (Fig. 10a). The resulting map of vulnerability (represented by V_{half} values; Fig. 10b) is similar to the map of socioeconomic resilience shown in Fig. 1: vulnerability is higher in the south and lower in the north, especially close to Manila.

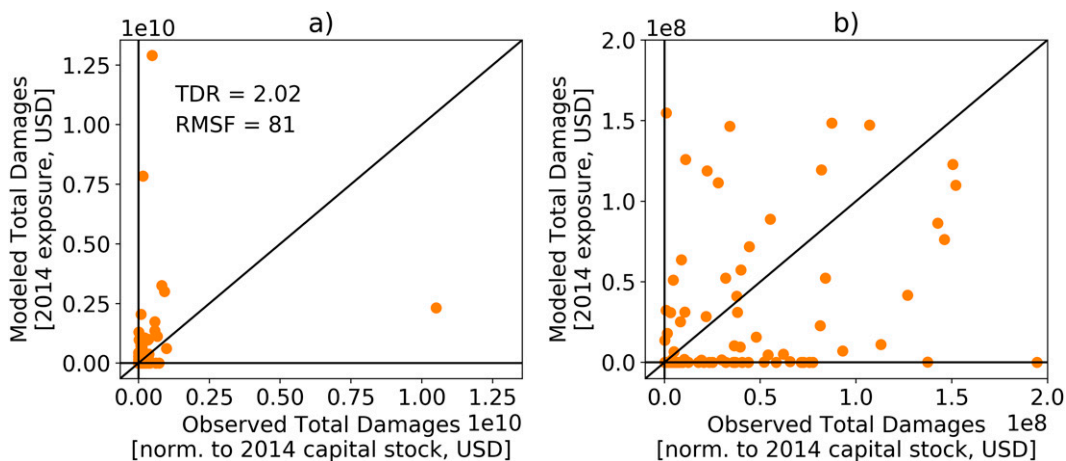


FIG. 11. Observed vs modeled damages for regionally varying vulnerability. (a) Observed total damages from EM-DAT plotted against modeled total damages calculated with the regional varying vulnerability map; black line is the one-to-one line; TDR and RMSF values calculated across all historical storms are shown in (a). (b) As in (a), but with reduced x- and y-axis limits to highlight the prevalence of storms with zero modeled damages.

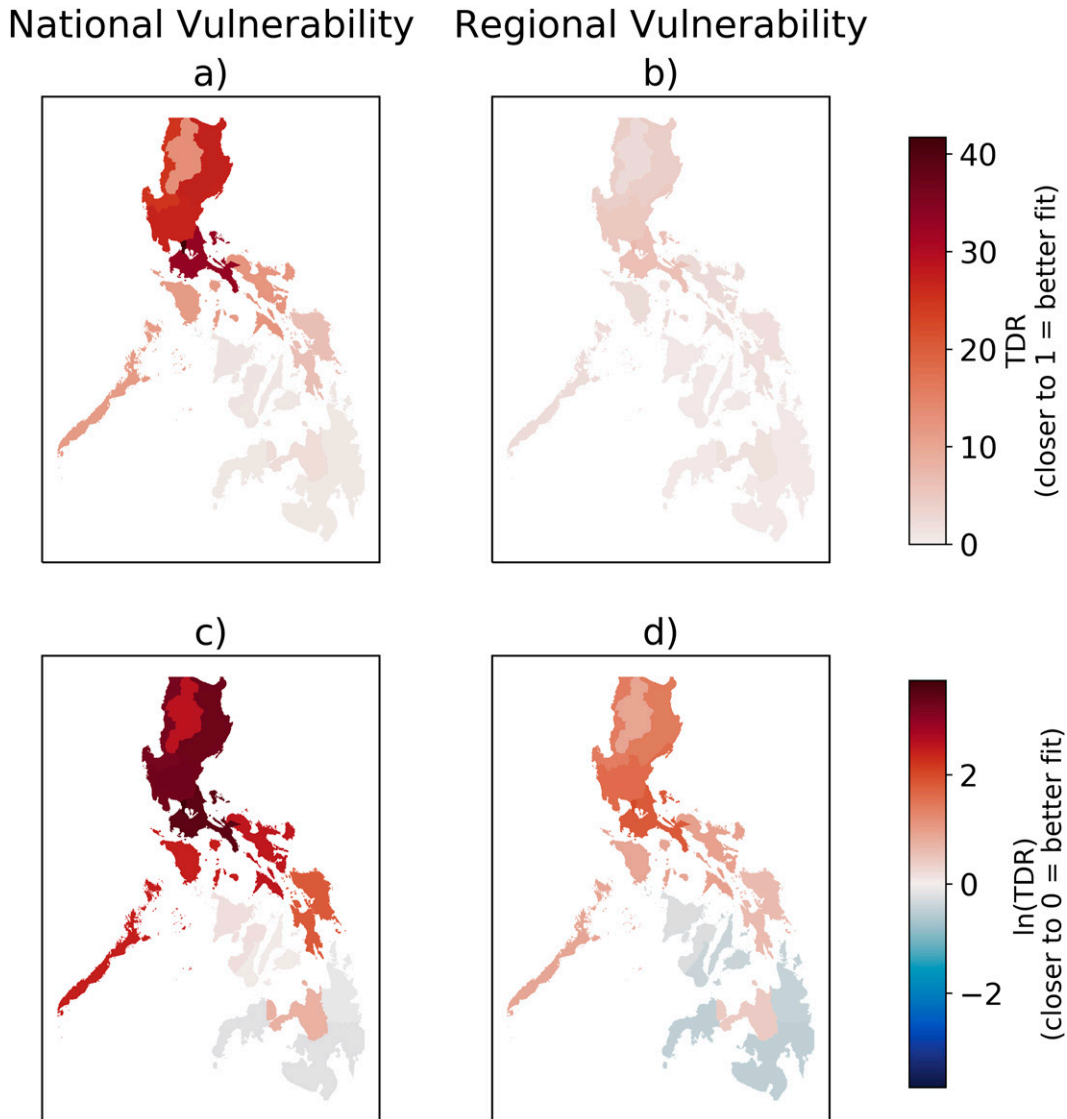


FIG. 12. Damage simulation skill for national vs regionally varying vulnerability. TDR across regions for (left) single national vulnerability curve and (right) regionally varying vulnerability curves and quantified as (top) raw TDR vs (bottom) natural log of TDR.

We employ this map of regional vulnerability to recalculate simulated damages for historical storms making landfall in the Philippines and compare to reported damages from EM-DAT. The results of this analysis are shown in Figs. 11 and 12. Compared to the nationally fit vulnerability curves minimizing RMSF (Fig. 8), the regionally varying vulnerability curves result in smaller RMSF (81 versus 92). Perhaps more striking, TDR is reduced from 9.28 to 2.02, even though TDR was not explicitly optimized for. For individual regions in the Philippines, TDR calculated for the subset of storms affecting each region is much improved as well. With a single national vulnerability curve, northern regions reach TDR values above 20 (Fig. 12). In contrast, considering regionally varying vulnerability curves leads to TDR values below 10 across the Philippines, and in most cases quite close to 1.

While key aspects of the simulated damages compare better to reported estimates with spatially varying vulnerability, as described above, others do not. In particular, with both versions of the vulnerability layer (national and regional) there are many storms with substantial reported damages that have zero simulated damages (Fig. 11b). This error likely represents a structural limitation of our risk model. Here we use wind as a proxy for all TC-related damages. However, other hazards associated with TCs (storm surge, flooding due to rainfall, landslides) may occur at relatively low wind speeds (e.g., lower than the V_{thresh} value of 25 m s^{-1} used in the vulnerability curve) and result in damages that our model does not capture.

As an illustrative example, simulated damages from Typhoons Haiyan (Yolanda) and Ketsana (Ondoy) are shown in Fig. 13. Our model simulates no damages resulting from Ketsana, though

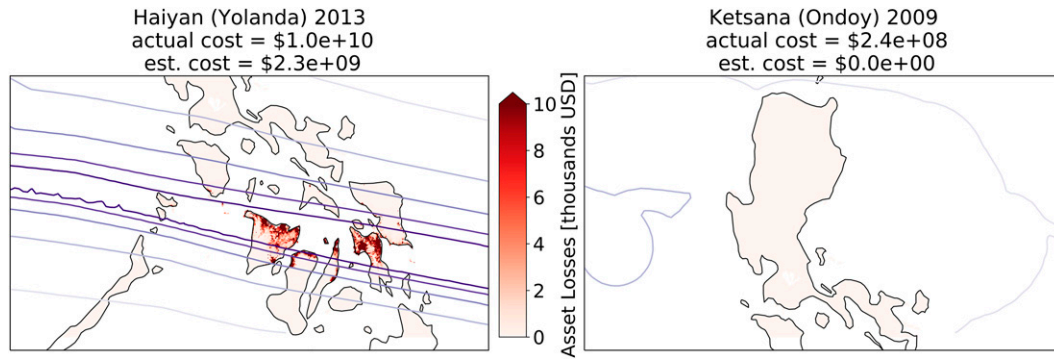


FIG. 13. Wind swath and asset losses for two notable Philippines-landfalling typhoons. Wind swath (contoured in purple; darker contours correspond to faster wind speeds) and damages (shaded red) for (left) Typhoon Haiyan (Yolanda) and (right) Typhoon Ketsana (Ondoy). The plot region is constrained to the area of most direct impact by each storm, and at the top of each plot the actual cost from EM-DAT is listed above the simulated damages summed across the entire Philippines.

it actually produced damages of \$240 million according to EM-DAT. This appears to be because Ketsana was a relatively weak storm (tropical storm intensity) in terms of wind speed when it affected the Philippines, with damages dominated by extreme rainfall and flash flooding (Sato and Nakasu 2011), processes our model does not represent in any explicit way. In contrast, our model does simulate billions of dollars' worth of damages from Typhoon Haiyan, though it underestimates those damages by a factor of 4.3. This may reflect the lack of explicit storm surge in our model, as a large fraction of the damages caused by Haiyan resulted from storm surge (Lagmay et al. 2015).

5. Return periods of TC risk in the Philippines

The goal of this work was to create a usable country and regional-scale TC risk model for the Philippines. Before concluding the paper, we briefly highlight the utility of our model for estimating TC risk return periods in the Philippines.

In assessing TC risk for diverse aspects of emergency preparedness, from building construction standards to emergency response plans, it is useful to know the expected frequency of events of a given severity. This is typically quantified as a return period (1/frequency) in units of years for a given event severity. Using our model, we can calculate return periods empirically for both wind speed and asset losses for different regions in the Philippines. The most accurate hazard input is obtained using historical TC tracks, but this allows estimation only of return periods several times shorter than the length of the historical record (76 years). Using our TC risk model run with CHAZ tracks allows consistent estimation of TC wind speed and asset losses out to much longer return periods. For CHAZ, we adjust the storm frequency such that the regional landfall rate per year in CHAZ is consistent with that of the historical record—that is, for each region,

$$\text{years}_{\text{CHAZ}} = \text{landfalls}_{\text{CHAZ}} / (\text{landfalls}_{\text{IBTrACS}} / \text{years}_{\text{IBTrACS}}), \quad (11)$$

which amounts to a regional-scale bias correction on the landfall rate. Resulting maps of wind speed and loss return levels

for regions across the Philippines are shown in Fig. 14. While higher winds speeds are experienced by the farthest north Philippines, the most dramatic increase in losses with return period occurs in the northern to central Philippines. This highlights the fundamentally different patterns of hazard versus economic risk and the utility of rigorously modeling such risk.

Examples of specific exceedance curves for NCR and Eastern Visayas are shown in Fig. 15. Both the advantages and challenges of our approach are clearly demonstrated in determining the return period for a Haiyan-like event in Eastern Visayas as shown in Fig. 15. Based on the historical record, in Eastern Visayas Typhoon Haiyan has a return period of about 70–80 years (since it occurred within the bounds of a historical record of approximately that length) but is clearly an outlier and not well constrained. The generalized Pareto distribution (GPD) fit presents a purely statistical means to extend the observed record to longer return periods and finds a slightly longer return period for Haiyan's hazard of about 100 years. In contrast, in the context of the much-larger sample of physically plausible TCs from CHAZ, the hazard associated with a Haiyan-like event has a return period of several thousand years, and the losses from such an event are outside the range of synthetic storms (e.g., return period greater than 10 000 years). In contrast to Eastern Visayas, in NCR the GPD fit and the CHAZ estimates are substantially better aligned for wind hazards.

It appears that the larger sample of storms from CHAZ may more robustly constrain the return period of Haiyan. CHAZ is advantageous over just the historical record in including more storms and is advantageous over the GPD fit in capturing dynamics important for storm genesis, intensification, and tracks that allow incorporation of changing background climate conditions. That said, there are important caveats to consider with this CHAZ-based estimate. CHAZ (like any model) may have biases—in Eastern Visayas, CHAZ-based asset losses appear to be biased somewhat too low given that the historical records lie slightly above the intensity ensemble (thin red lines). While we perform some light bias correction on the regional storm frequency (as

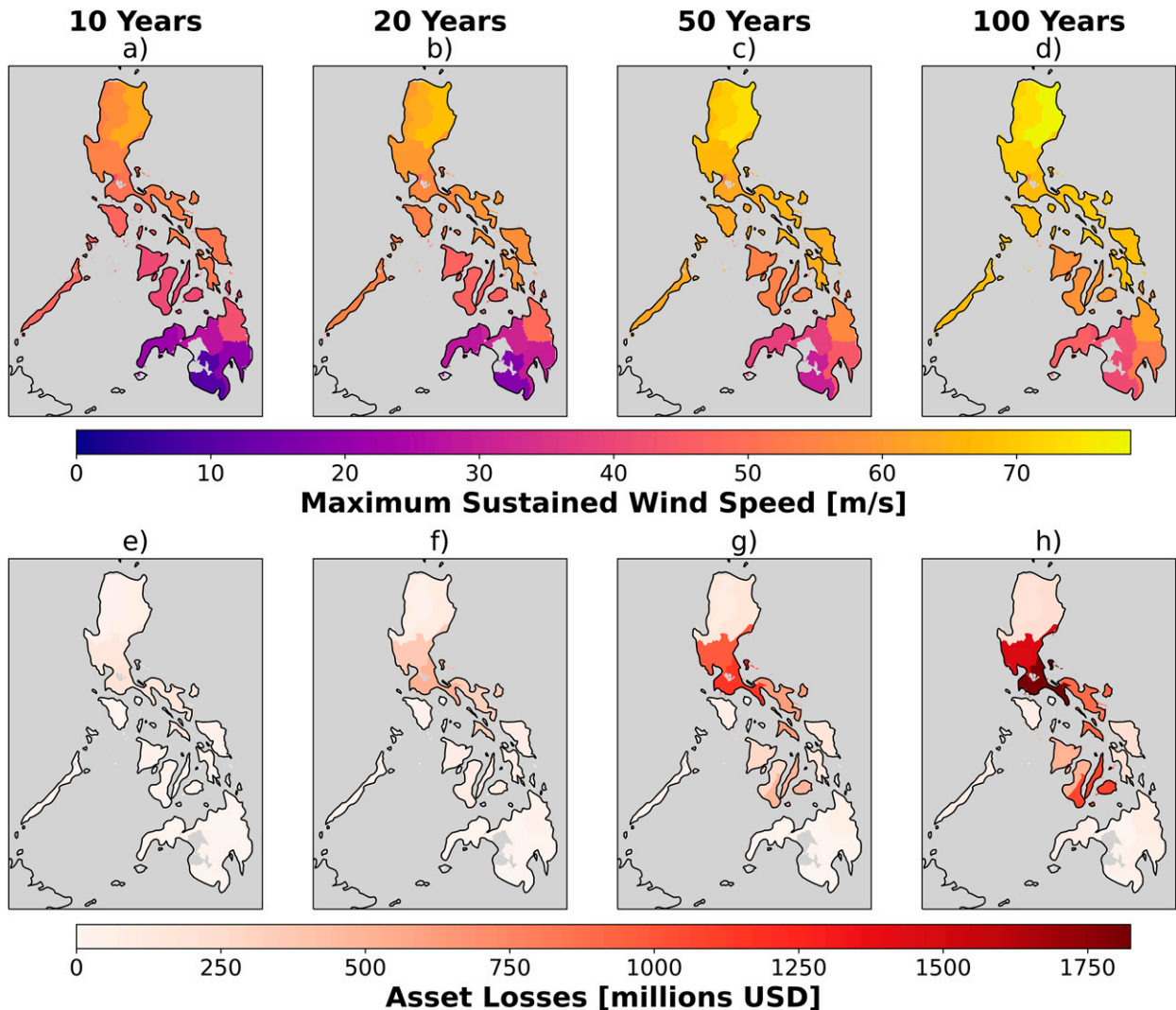


FIG. 14. Maps of return levels for wind speed and asset losses across all regions in the Philippines. Return levels of (top) maximum sustained wind speed and (bottom) asset losses are shown for (a),(e) 10-, (b),(f) 20-, (c),(g) 50-, and (d),(h) 100-yr return periods. Risk assessment is conducted using the synthetic CHAZ-based TC events. Values for the ARMM region are excluded because the adjustment of storm frequency [Eq. (11)] cannot be directly applied for a region that has no historical landfalling TCs.

mentioned in the prior paragraph), more intensive bias corrections could be applied, such as subselecting more realistic CHAZ tracks. Additionally, the CHAZ simulations here used environmental variables taken from the ERA-Interim reanalysis in the recent historical period, with all years treated the same in the return period calculation; thus, any possible climate change signal would be obscured to the extent that it might render 2013 (when Haiyan occurred) different than the earlier part of the period.

6. Discussion

In this study, we combined TC wind, exposed value, and regionally refined vulnerability calibrated on historical damages to estimate economic losses from TCs in the Philippines. The

model exhibits skill in assessing return levels of wind hazard and damages across populations of storms. However, this is nonetheless a less refined model compared to those used in proprietary applications where large amounts of claims data are available to constrain exposure and vulnerability, or as compared to FEMA’s Hazus model in the United States. In contrast to these more comprehensive models, the spirit of our approach is to see what is possible with openly available datasets common to many lower-income countries to take a step forward in open-source TC risk modeling. However, there are definite limitations to our approach. For example, we make the strong simplifying assumption that all damages can be modeled as proportional to wind, which leads our model to completely miss damages from some historically impactful weak-wind TCs that exhibited substantial flooding.

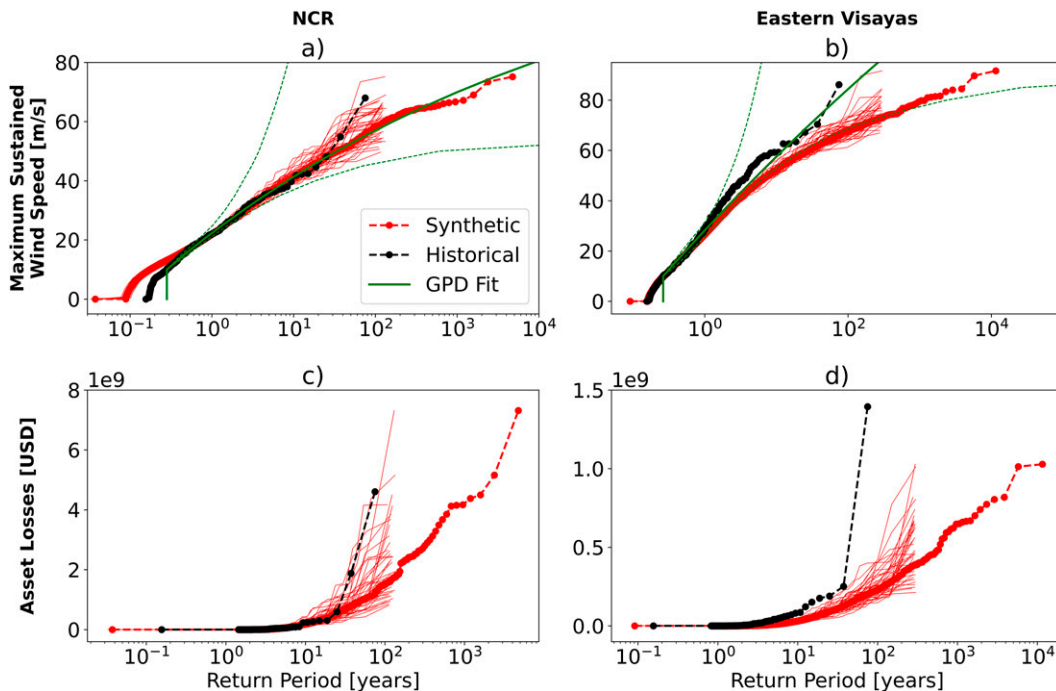


FIG. 15. Return periods for different levels of wind speed and asset losses in two Philippines regions. Return periods of different (top) maximum sustained wind speeds and (bottom) asset losses for two regions: (left) NCR and (right) Eastern Visayas. Simulated damages from IBTrACS tracks are shown in black, while simulated damages from CHAZ tracks are shown in red; thin red lines designate return periods derived from each CHAZ intensity ensemble, while the thick dashed red line shows return periods from all the CHAZ tracks and intensity ensembles together. In the top panels, the green lines represent the GPD fit to the historical IBTrACS-based windspeeds, with the solid line being the central estimate and the dashed lines demarcating the 90% confidence interval. For the GPD fit, events below a 10 m s^{-1} wind speed are excluded.

Uncertainties exist in all three layers of our model. First, the CHAZ wind tracks exhibit biases compared to observed storms making landfall in the Philippines and some strong landfalling TCs do not penetrate as far into the Philippines as observed (Fig. 3). While various bias-correction techniques (such as subsetting more realistic tracks) are possible to improve this issue, we tried to minimize bias correction in this work to provide a candid view of the current model ability to hopefully inspire future improvements. Second, our wind field modeling technique neglects some processes known to substantially effect wind fields, like boundary layer roughness, and assumes particular algorithms for asymmetry and decay profiles that could be varied. Third, the accuracy of the vulnerability layer is limited by the quality of losses from EM-DAT data, the number of damaging Philippines storms in the observed record, and the resolution and quality of the household survey data. Fourth, the exposed value dataset was developed for a large group of countries, and its underlying algorithms that relate population and night lights to exposed value could perhaps be better fit for the Philippines. Finally, both vulnerability and exposure layers are assumed static over time, whereas it is known that the population and economy grew over the historical period in the Philippines. Many of these uncertainties are not straightforward to quantitatively constrain, especially due to limitations of the available data.

As a result, a comprehensive uncertainty analysis is outside the scope of the present work but is an important area for future inquiry.

Many aspects of this model could be improved, and we highlight a few here. On the hazard front, modeling other TC-related hazards beyond wind could allow better simulation of impacts from many storms (Lin et al. 2010, 2012; Aerts et al. 2013; Rodrigo et al. 2018). At present, our model simulates zero damages for some historical TCs that did, in fact, produce damage. We believe this is because the damage from these storms was predominantly due to rainfall and flooding—hazards that are only indirectly, and very loosely, related to wind speed. Regarding the existing wind model, capturing surface roughness could allow more accurate simulation of wind speeds, and in turn damages, over land. We expect this limitation to be much less important than the omission of flooding, however, in part because our vulnerability curves are fit to the winds we use. The regional vulnerability approach can compensate further (compared to the national fit) for the lack of roughness in our model, as vulnerability is found to be lowest in urban regions where roughness would likely be decelerating surface winds to the greatest extent. The method of incorporating TC asymmetry here is also a relatively simple function of TC translation, which might be superseded in future model iterations by more advanced

methods (Lin and Chavas 2012; Chang et al. 2020; Yang et al. 2022).

There are many areas within the vulnerability and exposure modeling that merit further development as well. First, the temporal and spatial resolution of the vulnerability and exposure layers might be improved. Our assumption of static vulnerability and exposure was made largely due to data limitations—the exposure data that are presently available are calibrated for 2014, and the historical record of storms and reported damages is limited and varies substantially in density through time, with many more events later in the record. Thus, subdividing the data further to calibrate vulnerability at the regional level presented robustness issues. Satellite-based datasets and street-pose imagery, such as Google Street View, might present a useful way forward for generating more detailed vulnerability and exposure layers (e.g., province or even building scale) and capturing some trends through time (Kang et al. 2018; Ayush et al. 2020). Second, agricultural losses could be more rigorously quantified. At present, the exposure layer includes built assets but does not explicitly include agriculture. This may bias our results, as recorded agricultural losses have been significant in many historical Philippines TCs (ELB21). Third, appropriate values of the vulnerability parameter V_{thresh} might be more robustly determined, particularly in countries with a wide range of construction standards. Here we have focused primarily on fitting V_{half} , but our national vulnerability curve fitting results suggest that in some circumstances values of V_{thresh} higher or lower than that used here (25 m s^{-1} , similar with prior work) could be more accurate. This issue is perhaps particularly acute when wind is used as a proxy for all TC-related hazards, since substantial flooding can occur at relatively small wind speeds. Fourth, more work could be done to examine the causes of the regional variation in vulnerability. While we relate regional V_{thresh} values to a measure of the strength of roof construction materials, the positive relationship between these two quantities does not necessarily reflect stronger roofs directly reducing vulnerability. The proportion of strong roofs may simply correlate with other quantities that could reduce vulnerability, such as wealth and urbanization. Indeed, in some small island communities in the Philippines, light cogon roofs are actually reported to be adaptive to tropical cyclones as they can be tied down in high winds (Board 2019), highlighting a limitation of our focus on strong/heavy roofs to explain vulnerability.

7. Summary and conclusions

We have described the development and application of a TC risk model for the Philippines. This model includes three layers—hazard, exposure, and vulnerability—which, when combined, allow quantification of asset losses from storms. The present study focuses on the Philippines, but the methodology could be straightforwardly applied to other countries. Hazard is represented by swaths of maximum sustained wind speeds, derived from a parametric wind field model with a simple geometric correction for TC asymmetry. Swaths can be derived from observed TC tracks (e.g., IBTrACS) or synthetically generated TC tracks, such as from CHAZ. Exposure is derived from the existing LitPop dataset, which

distributes national total asset value across each country proportional to a combination of night lights and population data (Eberenz et al. 2020). For vulnerability, we employ the Emanuel (2011) functional form for vulnerability. However, we run a number of tests to fit the vulnerability curve parameters (V_{half} and V_{thresh}) to accurately simulate historical losses.

This work is novel in two main ways. First, while there are other existing TC risk models, this is the first attempt to use the open-source CHAZ model to quantify economic risks from TCs, opening the door for a variety of future applications. Most notable is the ability to estimate asset losses from TCs in the present and with climate change using open-source methods, especially in relatively data-poor countries like the Philippines. Second, we demonstrate the benefits of fitting regional (as opposed to national) vulnerability curves based on open-source economic data for TC risk analysis.

Initially, we tried fitting one vulnerability curve for the entire Philippines. Similar to results in ELB21, we find that this approach results in substantial uncertainty regarding the appropriate vulnerability curve. If the vulnerability is fit to best represent total damages (TDR close to 1), damages from TCs that pass through Manila are well simulated, while damages from other storms are underestimated. In contrast, if all storms are weighted equally in fitting vulnerability (RMSF minimized), damages from TCs that pass through Manila are substantially overestimated, and the TDR is approximately 9.

We hypothesized that this trade-off regarding the appropriate vulnerability curve resulted from urban–rural differences not captured by a national-scale vulnerability fit. We tried instead fitting V_{half} for each region to minimize RMSF based on the subset of historical storms that affected each region. The V_{half} values from this analysis suggest that Manila indeed has the lowest vulnerability in the Philippines. These parameter values were also found to be positively correlated with a proxy of structural vulnerability based on household survey data, namely, the proportion of strong to light roofs. Regressing V_{half} against this roof strength proportion, we determined V_{half} values for each region of the Philippines, and in so doing determined a regional map of TC vulnerability. Applying this regional TC vulnerability layer to simulate historical Philippines storms, we find lower RMSF, a TDR value across the Philippines of 2, and TDR values for individual provinces much closer to 1. We conclude that regional, and especially urban versus rural, differentiation of vulnerability is critical for accurate TC risk modeling in the Philippines.

The TC risk model presented here fulfills the primary goal of this study to develop methods for open-source TC risk modeling relevant in lower-income, data-limited countries. Our exposure and hazard methods are fully open source and could be adapted for any country. The vulnerability methods we developed rely on existing openly available damage data (EM-DAT), combined with household survey or census data, which is publicly available for many countries. Survey questions can vary by country, so our chosen vulnerability proxy of roof strength may not always be available, but we expect other questions related to house fragility or even family income can usefully serve as proxies for structural vulnerability. Altogether, these open-source methods and code increase

access to risk assessment resources generally reserved for wealthy countries, the reinsurance industry, and private capital.

This work also fulfills our secondary goal to produce a usable TC risk model for the Philippines. The present model exhibits significant skill in simulating aggregate damages across many storms and can be used to constrain return levels of wind hazards and asset losses. This type of risk assessment generates insights useful for all stages of disaster risk management policy dialogues. Expected asset losses are used in sovereign risk financing dialogues to define needs and insurance premiums. Simulations of extreme events are useful for assessing tail risks and compound shocks, relevant to macrofiscal and humanitarian contingency planning. Complex dynamics associated with economic and population growth and climate change present challenges for such planning in the Philippines. The open-source methods and code documented here allow more flexible risk assessment for the Philippines that can better account for such complexity. In particular, our model opens up the possibility of exploring expected asset losses under varying economic, population, and climate trajectories and assumptions.

Our study opens up a few key areas for further model development and application. Regarding model development, the current model quality encourages caution in interpreting results for individual storms that could be dominated by hazards other than wind; future model development should seek to add storm surge and precipitation subperils. In this study, we also treated each storm as independent in its hazard and damages—exploring temporal compounding of multiple storms would be an interesting extension to this work. Spatial and temporal detail of vulnerability and exposure layers could be substantially improved by building maps derived from satellite and street-pose imagery. Development of improved methods for quantifying and propagating uncertainties between the hazard, exposure, and vulnerability layers of the model would allow more comprehensive understanding of the drivers of uncertainty in the final risk assessment. We also intend to extend this model to assess TC impacts across the income distribution, which is useful for mapping and addressing vulnerabilities, and for crafting postdisaster assistance packages (Hallegatte et al. 2016; Walsh and Hallegatte 2020). We hope to apply the general methodology outlined here to other countries to work toward global TC risk assessments. Finally, we plan to estimate projected changes in TC risk with global warming by pairing this model with CHAZ tracks generated using environmental variables taken from climate change scenarios simulated with earth system models (Emanuel 2011; Lee et al. 2020); such results would be relevant to both adaptation planning and financial risk modeling, which regulations increasingly require to consider climate change (Fiedler et al. 2021).

Acknowledgments. We thank Samuel Eberenz, Olivia Cabrera, Dail Rowe, Kyle Mandli, and Stephane Hallegatte for useful conversations and feedback. We also thank Qidong Yang for sharing his implementation of the Willoughby wind profile model. Comments from two anonymous reviewers greatly improved the manuscript. J. W. B. was supported by the Lamont-Doherty

Earth Observatory Postdoctoral Fellowship. C. Y. L. and S. J. C. thank support from the Vetlesen Foundation to the Lamont-Doherty Earth Observatory of Columbia University. S. J. C., C. Y. L., and A. H. S. acknowledge support from the Swiss Re Foundation.

Data availability statement. Data and code supporting the analyses and figures in this publication are available through DesignSafe (<https://doi.org/10.17603/ds2-hsqp-k357>) and can be cited as Baldwin et al. (2023). The code supporting this publication is also available on GitHub at https://github.com/janewaldwin/TC_Risk_WorldBank. CHAZ is available on GitHub at <https://github.com/cl3225/CHAZ>. LitPop is available at <https://www.research-collection.ethz.ch/handle/20.500.11850/331316>. EM-DAT is available online at <https://public.emdat.be>.

REFERENCES

- Aerts, J. C. J. H., N. Lin, W. Botzen, K. Emanuel, and H. de Moel, 2013: Low-probability flood risk modeling for New York City. *Risk Anal.*, **33**, 772–788, <https://doi.org/10.1111/risa.12008>.
- Ayush, K., B. Uzgent, M. Burke, D. Lobell, and S. Ermon, 2020: Generating interpretable poverty maps using object detection in satellite images. arXiv, 2002.01612v2, <http://arxiv.org/abs/2002.01612>.
- Baldwin, J., C.-Y. Lee, B. Walsh, S. Camargo, and A. Sobel, 2023: Replication data for “Vulnerability in a tropical cyclone risk model: Philippines case study.” DesignSafe, accessed 12 February 2023, <https://doi.org/10.17603/ds2-hsqp-k357>.
- Bersales, L. G. S., 2017: 2015 Family Income and Expenditure Survey. Philippine Statistics Authority, 207 pp., <https://psa.gov.ph/sites/default/files/FIES%202015%20Final%20Report.pdf>.
- Beven, J. L., II, and Coauthors, 2008: Atlantic hurricane season of 2005. *Mon. Wea. Rev.*, **136**, 1109–1173, <https://doi.org/10.1175/2007MWR2074.1>.
- Bloemendaal, N., H. de Moel, S. Muis, I. D. Haigh, and J. C. J. H. Aerts, 2020a: Estimation of global tropical cyclone wind speed probabilities using the STORM dataset. *Sci. Data*, **7**, 377, <https://doi.org/10.1038/s41597-020-00720-x>.
- , I. D. Haigh, H. de Moel, S. Muis, R. J. Haarsma, and J. C. J. H. Aerts, 2020b: Generation of a global synthetic tropical cyclone hazard dataset using STORM. *Sci. Data*, **7**, 40, <https://doi.org/10.1038/s41597-020-0381-2>.
- Board, J., 2019: In the path of the storm: Life in Batanes on the Philippines’ typhoon track. *Channel News Asia*, 13 January, <https://www.channelnewsasia.com/asia/islands-in-the-path-of-typhoons-life-in-batanes-philippines-792076>.
- Chang, D., S. Amin, and K. Emanuel, 2020: Modeling and parameter estimation of hurricane wind fields with asymmetry. *J. Appl. Meteor. Climatol.*, **59**, 687–705, <https://doi.org/10.1175/JAMC-D-19-0126.1>.
- Chavas, D. R., and J. A. Knaff, 2022: A simple model for predicting the tropical cyclone radius of maximum wind from outer size. *Wea. Forecasting*, **37**, 563–579, <https://doi.org/10.1175/WAF-D-21-0103.1>.
- , N. Lin, and K. Emanuel, 2015: A model for the complete radial structure of the tropical cyclone wind field. Part I: Comparison with observed structure. *J. Atmos. Sci.*, **72**, 3647–3662, <https://doi.org/10.1175/JAS-D-15-0014.1>.

- Cinco, T. A., and Coauthors, 2016: Observed trends and impacts of tropical cyclones in the Philippines. *Int. J. Climatol.*, **36**, 4638–4650, <https://doi.org/10.1002/joc.4659>.
- Corporal-Lodangco, I. L., and L. M. Leslie, 2017: Climatology of Philippine tropical cyclone activity: 1945–2011. *Int. J. Climatol.*, **37**, 3525–3539, <https://doi.org/10.1002/joc.4931>.
- , —, and P. J. Lamb, 2016: Impacts of ENSO on Philippine tropical cyclone activity. *J. Climate*, **29**, 1877–1897, <https://doi.org/10.1175/JCLI-D-14-00723.1>.
- Cutter, S. L., B. J. Boruff, and W. L. Shirley, 2003: Social vulnerability to environmental hazards. *Soc. Sci. Quart.*, **84**, 242–261, <https://doi.org/10.1111/1540-6237.8402002>.
- Dee, D. P., and Coauthors, 2011: The ERA-Interim reanalysis: Configuration and performance of the data assimilation system. *Quart. J. Roy. Meteor. Soc.*, **137**, 553–597, <https://doi.org/10.1002/qj.828>.
- del Rosario, E. D., 2013: Final report re effects of Typhoon “Yolanda” (Haiyan). National Disaster Risk Reduction and Management Council, 148 pp., [https://ndrrmc.gov.ph/attachments/article/1329/FINAL_REPORT_re_Effects_of_Typhoon_YOLANDA_\(HAIYAN\)_06-09NOV2013.pdf](https://ndrrmc.gov.ph/attachments/article/1329/FINAL_REPORT_re_Effects_of_Typhoon_YOLANDA_(HAIYAN)_06-09NOV2013.pdf).
- Dominguez, C., A. Jaramillo, and P. Cuéllar, 2021: Are the socioeconomic impacts associated with tropical cyclones in Mexico exacerbated by local vulnerability and ENSO conditions? *Int. J. Climatol.*, **41**, E3307–E3324, <https://doi.org/10.1002/joc.6927>.
- Doxsey-Whitfield, E., K. MacManus, S. B. Adamo, L. Pistolesi, J. Squires, O. Borkovska, and S. R. Baptista, 2015: Taking advantage of the improved availability of census data: A first look at the gridded population of the world, version 4. *Pap. Appl. Geogr.*, **1**, 226–234, <https://doi.org/10.1080/23754931.2015.1014272>.
- Eadie, P., M. E. Atienza, and M. Tan-Mullins, 2020: Livelihood and vulnerability in the wake of Typhoon Yolanda: Lessons of community and resilience. *Nat. Hazards*, **103**, 211–230, <https://doi.org/10.1007/s11069-020-03984-z>.
- Eberenz, S., D. Stocker, T. Rössli, and D. N. Bresch, 2020: Asset exposure data for global physical risk assessment. *Earth Syst. Sci. Data*, **12**, 817–833, <https://doi.org/10.5194/essd-12-817-2020>.
- , S. Lüthi, and D. N. Bresch, 2021: Regional tropical cyclone impact functions for globally consistent risk assessments. *Nat. Hazards Earth Syst. Sci.*, **21**, 393–415, <https://doi.org/10.5194/nhess-21-393-2021>.
- Ehrhart, B., S. Mildenhall, A. Podlaha, and S. Bowen, 2014: Annual global climate and catastrophe report: Impact forecasting—2013. Aon Benfield Rep., 68 pp., https://preparecenter.org/wp-content/sites/default/files/annual_global_climate_and_catastrophe_report_2013.pdf.
- Elliott, R. J. R., E. Strobl, and P. Sun, 2015: The local impact of typhoons on economic activity in China: A view from outer space. *J. Urban Econ.*, **88**, 50–66, <https://doi.org/10.1016/j.jue.2015.05.001>.
- Emanuel, K., 2005: Increasing destructiveness of tropical cyclones over the past 30 years. *Nature*, **436**, 686–688, <https://doi.org/10.1038/nature03906>.
- , 2011: Global warming effects on U.S. hurricane damage. *Wea. Climate Soc.*, **3**, 261–268, <https://doi.org/10.1175/WCAS-D-11-00007.1>.
- , R. Sundararajan, and J. Williams, 2008: Hurricanes and global warming: Results from downscaling IPCC AR4 simulations. *Bull. Amer. Meteor. Soc.*, **89**, 347–368, <https://doi.org/10.1175/BAMS-89-3-347>.
- Ericta, C. N., and E. Fabian, 2009: A documentation of the Philippines’ Family Income and Expenditure Survey. Working Paper 2009-18, PIDS Discussion Paper Series, 38 pp., <https://www.pids.gov.ph/publication/discussion-papers/a-documentation-of-the-philippines-family-income-and-expenditure-survey>.
- Feenstra, R. C., R. Inklaar, and M. P. Timmer, 2015: The next generation of the Penn World Table. *Amer. Econ. Rev.*, **105**, 3150–3182, <https://doi.org/10.1257/aer.20130954>.
- Fiedler, T., A. J. Pitman, K. Mackenzie, N. Wood, C. Jakob, and S. E. Perkins-Kirkpatrick, 2021: Business risk and the emergence of climate analytics. *Nat. Climate Change*, **11**, 87–94, <https://doi.org/10.1038/s41558-020-00984-6>.
- Field, C. B., and Coauthors, Eds., 2012: *Managing the Risks of Extreme Events and Disasters to Advance Climate Change Adaptation*. Cambridge University Press, 582 pp.
- Geiger, T., K. Frieler, and D. N. Bresch, 2018: A global historical data set of tropical cyclone exposure (TCE-DAT). *Earth Syst. Sci. Data*, **10**, 185–194, <https://doi.org/10.5194/essd-10-185-2018>.
- Gori, A., N. Lin, D. Xi, and K. Emanuel, 2022: Tropical cyclone climatology change greatly exacerbates US extreme rainfall–surge hazard. *Nat. Climate Change*, **12**, 171–178, <https://doi.org/10.1038/s41558-021-01272-7>.
- Guha-Sapir, D., R. Below, and P. Hoyois, 2009: EM-DAT: The International Disaster Database. Centre for Research on the Epidemiology of Disasters, accessed 3 April 2022, www.emdat.be.
- Hallegatte, S., A. Vogt-Schilb, M. Bangalore, and J. Rozenberg, 2016: Unbreakable: Building the resilience of the poor in the face of natural disasters. World Bank Rep. 110618, 201 pp., <https://documents1.worldbank.org/curated/en/512241480487839624/pdf/110618-PUB-Box396333B-PUBLIC-PUBDATE-11-24-16-UNIT-ITSKI.pdf>.
- Holland, G. J., 1980: An analytic model of the wind and pressure profiles in hurricanes. *Mon. Wea. Rev.*, **108**, 1212–1218, [https://doi.org/10.1175/1520-0493\(1980\)108<1212:AAMOTW>2.0.CO;2](https://doi.org/10.1175/1520-0493(1980)108<1212:AAMOTW>2.0.CO;2).
- Holmes, J. D., 1982: *Wind Pressures on Houses with High Pitched Roofs*. James Cook University of North Queensland, 78 pp.
- Hsu, S. A., and Z. Yan, 1998: A note on the radius of maximum wind for hurricanes. *J. Coastal Res.*, **14**, 667–668.
- Jayasinghe, N. C., J. D. Ginger, D. J. Henderson, and G. R. Walker, 2018: Distribution of wind loads in metal-clad roofing structures. *J. Struct. Eng.*, **144**, 04018014, [https://doi.org/10.1061/\(ASCE\)ST.1943-541X.0001992](https://doi.org/10.1061/(ASCE)ST.1943-541X.0001992).
- Jing, R., and N. Lin, 2020: An environment-dependent probabilistic tropical cyclone model. *J. Adv. Model. Earth Syst.*, **12**, e2019MS001975, <https://doi.org/10.1029/2019MS001975>.
- Kang, J., M. Körner, Y. Wang, H. Taubenböck, and X. X. Zhu, 2018: Building instance classification using street view images. *ISPRS J. Photogramm. Remote Sens.*, **145**, 44–59, <https://doi.org/10.1016/j.isprsjprs.2018.02.006>.
- Klotz, B. W., and H. Jiang, 2017: Examination of surface wind asymmetries in tropical cyclones. Part I: General structure and wind shear impacts. *Mon. Wea. Rev.*, **145**, 3989–4009, <https://doi.org/10.1175/MWR-D-17-0019.1>.
- Knaff, J. A., S. P. Longmore, R. T. DeMaria, and D. A. Molenaar, 2015: Improved tropical-cyclone flight-level wind estimates using routine infrared satellite reconnaissance. *J. Appl. Meteor. Climatol.*, **54**, 463–478, <https://doi.org/10.1175/JAMC-D-14-0112.1>.
- Knapp, K. R., M. C. Kruk, D. H. Levinson, H. J. Diamond, and C. J. Neumann, 2010: The International Best Track Archive

- for Climate Stewardship (IBTrACS): Unifying tropical cyclone data. *Bull. Amer. Meteor. Soc.*, **91**, 363–376, <https://doi.org/10.1175/2009BAMS2755.1>.
- Knutson, T., and Coauthors, 2020: Tropical cyclones and climate change assessment: Part II: Projected response to anthropogenic warming. *Bull. Amer. Meteor. Soc.*, **101**, E303–E322, <https://doi.org/10.1175/BAMS-D-18-0194.1>.
- Lagmay, A. M. F., and Coauthors, 2015: Devastating storm surges of Typhoon Haiyan. *Int. J. Disaster Risk Reduct.*, **11**, 1–12, <https://doi.org/10.1016/j.ijdrr.2014.10.006>.
- Lee, C.-Y., M. K. Tippett, A. H. Sobel, and S. J. Camargo, 2016: Autoregressive modeling for tropical cyclone intensity climatology. *J. Climate*, **29**, 7815–7830, <https://doi.org/10.1175/JCLI-D-15-0909.1>.
- , —, —, and —, 2018: An environmentally forced tropical cyclone hazard model. *J. Adv. Model. Earth Syst.*, **10**, 223–241, <https://doi.org/10.1002/2017MS001186>.
- , S. J. Camargo, A. H. Sobel, and M. K. Tippett, 2020: Statistical–dynamical downscaling projections of tropical cyclone activity in a warming climate: Two diverging genesis scenarios. *J. Climate*, **33**, 4815–4834, <https://doi.org/10.1175/JCLI-D-19-0452.1>.
- , A. H. Sobel, S. J. Camargo, M. K. Tippett, and Q. Yang, 2022: New York State hurricane hazard: History and future projections. *J. Appl. Meteor. Climatol.*, **61**, 613–629, <https://doi.org/10.1175/JAMC-D-21-0173.1>.
- Leitch, C., J. Ginger, B. Harper, P. Kim, N. Jayasinghe, and L. Somerville, 2010: Performance of housing in Brisbane following storms on 16 November 2008. *Aust. J. Struct. Eng.*, **11**, 45–62, <https://doi.org/10.1080/13287982.2010.11465055>.
- Lin, I.-I., I.-F. Pun, and C.-C. Lien, 2014: “Category-6” Super-typhoon Haiyan in global warming hiatus: Contribution from subsurface ocean warming. *Geophys. Res. Lett.*, **41**, 8547–8553, <https://doi.org/10.1002/2014GL061281>.
- Lin, N., and D. Chavas, 2012: On hurricane parametric wind and applications in storm surge modeling. *J. Geophys. Res.*, **117**, D09120, <https://doi.org/10.1029/2011JD017126>.
- Lin, N., K. A. Emanuel, J. A. Smith, and E. Vanmarcke, 2010: Risk assessment of hurricane storm surge for New York City. *J. Geophys. Res.*, **115**, D18121, <https://doi.org/10.1029/2009JD013630>.
- Lin, N., K. A. Emanuel, M. Oppenheimer, and E. Vanmarcke, 2012: Physically based assessment of hurricane surge threat under climate change. *Nat. Climate Change*, **2**, 462–467, <https://doi.org/10.1038/nclimate1389>.
- Lyon, B., and S. J. Camargo, 2009: The seasonally-varying influence of ENSO on rainfall and tropical cyclone activity in the Philippines. *Climate Dyn.*, **32**, 125–141, <https://doi.org/10.1007/s00382-008-0380-z>.
- Mas, E., J. Bricker, S. Kure, B. Adriano, C. Yi, A. Suppasri, and S. Koshimura, 2015: Field survey report and satellite image interpretation of the 2013 Super Typhoon Haiyan in the Philippines. *Nat. Hazards Earth Syst. Sci.*, **15**, 805–816, <https://doi.org/10.5194/nhess-15-805-2015>.
- Meecham, D., D. Surry, and A. G. Davenport, 1991: The magnitude and distribution of wind-induced pressures on hip and gable roofs. *J. Wind Eng. Ind. Aerodyn.*, **38**, 257–272, [https://doi.org/10.1016/0167-6105\(91\)90046-Y](https://doi.org/10.1016/0167-6105(91)90046-Y).
- Meiler, S., T. Vogt, N. Bloemendaal, A. Ciullo, C.-Y. Lee, S. J. Camargo, K. Emanuel, and D. N. Bresch, 2022: Intercomparison of regional loss estimates from global synthetic tropical cyclone models. *Nat. Commun.*, **13**, 6156, <https://doi.org/10.1038/s41467-022-33918-1>.
- Ribera, P., R. García-Herrera, and L. Gimeno, 2008: Historical deadly typhoons in the Philippines. *Weather*, **63**, 194–199, <https://doi.org/10.1002/wea.275>.
- Rodrigo, S. M. T., C. L. Villanoy, J. C. Briones, P. H. T. Bilgera, O. C. Cabrera, and G. T. T. Narisma, 2018: The mapping of storm surge-prone areas and characterizing surge-producing cyclones in Leyte Gulf, Philippines. *Nat. Hazards*, **92**, 1305–1320, <https://doi.org/10.1007/s11069-018-3252-9>.
- Román, M. O., and Coauthors, 2018: NASA’s Black Marble nighttime lights product suite. *Remote Sens. Environ.*, **210**, 113–143, <https://doi.org/10.1016/j.rse.2018.03.017>.
- Sato, T., and T. Nakasu, 2011: 2009 Typhoon Ondoy flood disasters in metro Manila. Natural Disaster Research Rep. 45, 12 pp., https://dil-opac.bosai.go.jp/publication/nied_natural_disaster/pdf/45/45-04E.pdf.
- Sobel, A. H., C.-Y. Lee, S. J. Camargo, K. T. Mandli, K. A. Emanuel, P. Mukhopadhyay, and M. Mahakur, 2019: Tropical cyclone hazard to Mumbai in the recent historical climate. *Mon. Wea. Rev.*, **147**, 2355–2366, <https://doi.org/10.1175/MWR-D-18-0419.1>.
- Soria, J. L. A., and Coauthors, 2016: Repeat storm surge disasters of Typhoon Haiyan and its 1897 predecessor in the Philippines. *Bull. Amer. Meteor. Soc.*, **97**, 31–48, <https://doi.org/10.1175/BAMS-D-14-00245.1>.
- Strobl, E., 2011: The economic growth impact of hurricanes: Evidence from U.S. coastal counties. *Rev. Econ. Stat.*, **93**, 575–589, https://doi.org/10.1162/REST_a_00082.
- Tellman, B., C. Schank, B. Schwarz, P. D. Howe, and A. de Sherbinin, 2020: Using disaster outcomes to validate components of social vulnerability to floods: Flood deaths and property damage across the USA. *Sustainability*, **12**, 6006, <https://doi.org/10.3390/su12156006>.
- Uhlhorn, E. W., B. W. Klotz, T. Vukicevic, P. D. Reasor, and R. F. Rogers, 2014: Observed hurricane wind speed asymmetries and relationships to motion and environmental shear. *Mon. Wea. Rev.*, **142**, 1290–1311, <https://doi.org/10.1175/MWR-D-13-00249.1>.
- United Nations Office for the Coordination of Humanitarian Affairs, 2022: Philippines: Super Typhoon Rai (Odette). OCHA Situation Rep. 7, 12 pp., <https://reliefweb.int/report/philippines/philippines-super-typhoon-rai-odette-situation-report-no-7-25-march-2022>.
- Vickery, P. J., J. Lin, P. F. Skerlj, L. A. Twisdale Jr., and K. Huang, 2006a: HAZUS-MH hurricane model methodology. I: Hurricane hazard, terrain, and wind load modeling. *Nat. Hazards Rev.*, **7**, 82–93, [https://doi.org/10.1061/\(ASCE\)1527-6988\(2006\)7:2\(82\)](https://doi.org/10.1061/(ASCE)1527-6988(2006)7:2(82)).
- , P. F. Skerlj, J. Lin, L. A. Twisdale Jr., M. A. Young, and F. M. Lavelle, 2006b: HAZUS-MH hurricane model methodology. II: Damage and loss estimation. *Nat. Hazards Rev.*, **7**, 94–103, [https://doi.org/10.1061/\(ASCE\)1527-6988\(2006\)7:2\(94\)](https://doi.org/10.1061/(ASCE)1527-6988(2006)7:2(94)).
- Walsh, B., and S. Hallegatte, 2019: Measuring natural risks in the Philippines: Socioeconomic resilience and wellbeing losses. World Bank Working Paper 8723, 62 pp., <https://openknowledge.worldbank.org/server/api/core/bitstreams/e5616b09-a7bd-5509-a271-b4db9e8af5a7/content>.
- , and —, 2020: Measuring natural risks in the Philippines: Socioeconomic resilience and wellbeing losses. *Econ. Disaster Climate Change*, **4**, 249–293, <https://doi.org/10.1007/s41885-019-00047-x>.

- Watson, C. C., Jr., and M. E. Johnson, 2004: Hurricane loss estimation models: Opportunities for improving the state of the art. *Bull. Amer. Meteor. Soc.*, **85**, 1713–1726, <https://doi.org/10.1175/BAMS-85-11-1713>.
- Willoughby, H. E., R. W. R. Darling, and M. E. Rahn, 2006: Parametric representation of the primary hurricane vortex. Part II: A new family of sectionally continuous profiles. *Mon. Wea. Rev.*, **134**, 1102–1120, <https://doi.org/10.1175/MWR3106.1>.
- Wilson, K. M., J. W. Baldwin, and R. M. Young, 2022: Estimating tropical cyclone vulnerability: A review of different open-source approaches. *Hurricane Risk in a Changing Climate*, J. M. Collins and J. M. Done, Eds., Vol. 2, *Hurricane Risk*, Springer International Publishing, 255–281.
- World Bank, 2021: Wealth accounting. World Bank, accessed 3 April 2022, <https://datacatalog.worldbank.org/search/dataset/0042066>.
- Xi, D., N. Lin, and J. Smith, 2020: Evaluation of a physics-based tropical cyclone rainfall model for risk assessment. *J. Hydrometeor.*, **21**, 2197–2218, <https://doi.org/10.1175/JHM-D-20-0035.1>.
- Yamin, L. E., A. I. Hurtado, A. H. Barbat, and O. D. Cardona, 2014: Seismic and wind vulnerability assessment for the GAR-13 global risk assessment. *Int. J. Disaster Risk Reduct.*, **10**, 452–460, <https://doi.org/10.1016/j.ijdrr.2014.05.007>.
- Yang, Q., C.-Y. Lee, M. K. Tippett, D. R. Chavas, and T. R. Knutson, 2022: Machine learning–based hurricane wind reconstruction. *Wea. Forecasting*, **37**, 477–493, <https://doi.org/10.1175/WAF-D-21-0077.1>.